Temperature elevation synergises with and enhances the type-I IFN-mediated restriction of MPXV

Chris Davis[1], Ilaria Epifano[1], Kieran Dee[1], Steven McFarlane[1], Joanna K. Wojtus, Benjamin Brennan[1], Quan Gu[1], Vattipally B. Sreenu[1], Kyriaki Nomikou[1], Lily Tong[1], Lauren Orr[1], Ana Da Silva Filipe[1], David A. Barr[2], Antonia Ho[1/2], Emma C. Thomson[1], Chris Boutell[1*].

[1] MRC-University of Glasgow Centre for Virus Research (CVR), Glasgow, Scotland (UK)
[2] Department of Infectious Diseases, Queen Elizabeth University Hospital, Glasgow, Scotland (UK)

*chris.boutell@glasgow.ac.uk

Running title: Temperature elevation inhibits monkeypox virus replication

Abstract

Fever is an evolutionary conserved host pro-inflammatory immune response that governs the regulation of multiple biological processes to control the outcome of infection. In January 2022, the World Health Organization (WHO) reported a global outbreak in mpox cases with a high incidence of human-to-human transmission. A frequent prodromal symptom of monkeypox virus (MPXV) infection is fever, with a febrile temperature range of 38.3 to 40.5 °C. However, the outcome of temperature elevation on MPXV infection remains poorly defined. Here, we isolated a circulating strain of MPXV from a patient who presented with fever (38.5 °C) and rash from the 2022 outbreak. Genomic sequencing identified this isolate to belong to the epidemic Clade IIb.B1. Transcriptomic analysis of infected cells demonstrated this virus to induce a strong IL6 pro-inflammatory immune response, consistent with a role for this pyrogen in the regulation of fever. We identify host-cell temperature at both physiological skin (33 °C) and clinical febrile temperatures (38.5 and 40 °C) to be a key determinant in the outcome of infection through the differential regulation of MPXV transcription and associated amplitude of host cytokine response to infection. Incubation of infected cells at 38.5 or 40 °C led to a restriction or ablation in MPXV replication, respectively. Importantly, this thermal inhibition was reversible upon temperature downshift to 37 °C without detriment to viral replication fitness. Co-stimulation of the type-I interferon (IFN) response led to a dose- and temperature-dependent inhibition in MPXV replication that restricted the re-establishment of infection upon temperature downshift and withdrawal of IFN as an immune stimulus. Our data identify febrile temperatures associated with mpox disease to be a critical component of the host pro-inflammatory immune response to infection which can synergise with the type-I IFN response to enhance the host-cell mediated restriction of MPXV.

Introduction

MPXV belongs to the Orthopoxvirus (OPXV) genus[1], which includes variola virus (VARV, the causative agent of smallpox) and vaccinia virus (VACV, the foundation virus of the smallpox vaccine). Since January 2022, the World Health Organization (WHO) reported a global rise in the number of confirmed mpox cases across all six WHO regions (> 90,000 confirmed cases and ≥ 150 deaths; September 2023), including previous non-endemic regions of Europe and the Americas (https://worldhealthorg.shinyapps.io/mpx_global/). While the natural zoonotic reservoir of MPXV is likely to be in small rodents[2-4], increased human-to-

human transmission has been widely reported during the 2022/23 outbreak and linked to the emergence of novel Clade IIb variants since 2016[5-7]. This has raised concern that MPXV may establish a global foothold in the human population due to waning levels of cross-protecting immunity conferred previously through smallpox vaccination[8,9].

Human-to-human transmission of MPXV occurs through close contact with infectious skin lesions, bodily fluids, or large respiratory droplets[3,4]. The spectrum of mpox disease is often variable and ranges from self-limiting disease in healthy immunocompetent adults to fatality in 1 to 10 % of affected individuals[10]. Common prodrome symptoms include fever, lymphadenopathy, pharyngitis, headache, and myalgia, followed by rash and skin lesions on the body, face, and genitals[8,10-13]. More than 70 % of confirmed cases report fever, with a febrile temperature range of 38.3 to 40.5 °C[11,14-17]. Fever is an evolutionary conserved host response to infection and inflammation that can influence multiple cellular processes, including host immunological responses to infection[18,19]. Body temperature varies throughout the day, with age, sex, and ethnic origin being contributing factors[20,21]. Unlike heat stroke or hyperthermia, fever represents a controlled shift in body temperature activated in response to exogenous (microbial) and endogenous (host) pyrogenic factors[20-22]. Clinical febrile temperatures can vary (ΔT of 1 to 4 °C above baseline); with low (38 to 39 °C), moderate (39.1 to 40 °C), high (40.1 to 41 °C), and hyperpyrexia (> 41.1 °C) temperature ranges[21]. Experimental evidence has shown tissue temperature to play a key role during viral infection and the induction of interferon (IFN)-mediated antiviral innate immune defences to infection[23-26]. Notably, antipyretic treatment of intensive care patients infected with influenza A virus (IAV) has been linked to increased patient mortality[27-29], suggesting a beneficial role of the fever response to protect against infection in a clinical setting.

While small animal and non-human primate (NHP) models have shown MPXV infection to induce fever[30-32], few studies have directly examined the influence of temperature on the outcome of infection. Historical evidence (circa 1960s) has shown divergent OPXVs to have variable ceiling temperatures of pox formation in chick embryos, with mpox restriction observed at temperatures ≥ 39.5 °C[33,34]. These findings suggest that tissue temperature is likely to play a key determinant in the replication and/or immunopathology of MPXV. However, *in vitro* studies have focused on laboratory-adapted strains of VACV, which are known to carry strain-specific mutations that can influence their thermal- and/or immuno-regulatory properties[22,35-38]. Thus, the influence of temperature elevation to control the outcome of OPXV infection remains poorly defined, specifically in circulating Clades or

99 strains of human origin. We therefore set out to investigate the net effect of temperature
100 elevation on the replication of MPXV using a clinical isolate derived from the 2022/23
101 outbreak.
102 We isolated a circulating strain of MPXV from a febrile hospitalised patient during
103 the 2022 outbreak, who was recruited to the International Severe Acute Respiratory and
104 Emerging Infections Consortium Comprehensive Clinical Characterisation Collaboration
105 (ISARIC4C) study (ISRCTN66726260). Genomic sequencing demonstrated this isolate
106 belonged to the Clade IIb.B1 epidemic strain. We demonstrate basal tissue and host-cell
107 temperature to be a key determinant in the outcome of MPXV infection at both physiological
108 skin temperature (33 °C) and clinical febrile (38.5 and 40 °C) temperatures relative to core
109 body temperature (37 °C). Incubation of infected cells at 40 °C led to an ablation in MPXV
110 replication. We show this thermal restriction to occur via a genome wide suppression in viral
111 transcription, with multiple viral open reading frames (ORFs) displaying temperature-
112 dependent profiles of differential gene expression (DEG). Importantly, we show that the
113 thermal restriction of MPXV is reversible upon temperature downshift to 37 °C without
114 impairment to viral replication fitness. Co-stimulation of the type-I IFN response led to a
115 dose- and temperature-dependent IFN-mediated restriction in MPXV replication that
116 attenuated the re-establishment of infection upon thermal downshift. Our data identify a
117 cooperative and synergistic role for temperature elevation to enhance the type-I IFN-
118 mediated restriction of MPXV. Findings pertinent to the immunological regulation of many
119 clinical pathogens that induce a fever response.
120

121 ## Results

122 **Temperature elevation inhibits MPXV replication in a cell-type dependent manner.**
123 We isolated a clinical strain of MPXV from a PCR positive patient presenting with fever
124 (38.5 °C), cough, myalgia, and rash. Illumina sequencing of inactivated clinical swabs
125 (CVR_MPXV1a) and infectious cell culture supernatant derived from primary amplification
126 (MPXV CVR_S1) identified an identical MPXV genome (accession number ON808413)
127 (Fig 1A). Phylogenetic analysis identified this virus to belong to the MPXV Clade IIb.B1
128 lineage and to contain 67 single nucleotide polymorphisms (SNPs) relative to the MPXV
129 Clade II reference strain (NC_063383). SNPs were located across the genome and present in
130 both core and accessory ORFs. Consistent with previous MPXV Clade IIb genomic

131 analysis[7,39,40], 91% of the SNPs (61 out of 67 nucleotides) were consistent with APOBEC
132 deamination (G to A or C to T substitutions; Fig 1B).
133 As MPXV CVR_S1 (here after referred to as MPXV) was isolated from a patient with
134 fever, we next investigated the influence of tissue temperature on MPXV replication in skin
135 epithelium. Human keratinocytes were differentiated into a pseudostratified epithelium under
136 air liquid interface (ALI). Tissues were mock treated or infected with MPXV (10^2 or 10^3
137 plaque-forming units (PFU)/tissue) at 37 °C for 1 h prior to continued incubation at 33, 37, or
138 40 °C (representative of skin, core, and maximum clinical febrile temperature range,
139 respectively) for 72 h. Haematoxylin and eosin (H&E) staining of mock treated tissue
140 sections demonstrated no significant difference in skin epithelium thickness, morphology, or
141 integrity over the temperature range of analysis (Fig 2A, B; Fig S1). As expected,
142 immunohistochemistry (IHC) staining of tissue sections identified MPXV virion antigen
143 expression to increase in a multiplicity of infection (MOI) dependent manner at 33 and 37 °C
144 (Fig 2A; Fig S1). Notably, discrete foci of infection could be observed at both temperatures,
145 indicative of MPXV intraepithelial propagation and spread at 72 h (Fig 2A; 10^2 PFU/tissue).
146 Quantitation of IHC stained tissue sections demonstrated the relative levels of MPXV
147 infection to be dependent on incubation temperature, with the highest levels of replication
148 observed at 37 °C (Fig 2C, D). Importantly, a significant reduction in MPXV antigen staining
149 could be observed at both physiological skin (37 *vs*. 33 °C) and febrile (37 *vs.* 40 °C)
150 incubation temperatures, with MPXV staining at 40 °C close to background levels observed
151 in mock treated samples (Fig 2A, C, D). Together, these data identify tissue temperature to
152 play a key determinant in the outcome of MPXV replication at both physiological and febrile
153 temperature ranges associated with clinical infection.
154 To examine the influence of temperature on the replication kinetics of MPXV in more
155 detail, we next compared the thermal sensitivity of MPXV to that of VACV (strain WR;
156 internal positive control)[38]. Human foreskin fibroblast (HFt) cells were infected at 37 °C for 1
157 h prior to incubation at 33, 37, 38.5 or 40 °C (representative of skin, core, and low to
158 moderate grade febrile temperature ranges, respectively). Infected monolayers were fixed at
159 48 h and analysed for viral plaque formation by Coomassie staining. Consistent with previous
160 results[38], VACV demonstrated a significant decrease in plaque number, plaque size, and titre
161 of cell-released virus (CRV) at incubation temperatures > 37 °C (Fig 3A to D). Notably,
162 plaque formation could still be observed at 40 °C, demonstrating the inhibitory ceiling
163 temperature for VACV had yet to be reached (Fig 3A, B)[38]. A significant reduction in plaque
164 size and CRV titre could also be observed upon incubation at 33 °C (Fig 3C, D),

165 demonstrating physiological temperatures below 37 °C to be inhibitory to optimal VACV
166 replication. qPCR analysis of intracellular viral DNA (vDNA) levels harvested at 2 h post-
167 infection (hpi; 1 h post-temperature shift) demonstrated the thermal restriction of VACV to
168 occur independently of a block to virus entry (Fig 3E). Moreover, no significant difference in
169 cell number, cell viability, or puromycin-induced cell death (positive control) was detected in
170 mock treated cells at 40 °C relative to incubation at 37 °C (Fig S2A, B), confirming cell
171 monolayer health and responsiveness to stimuli at temperatures > 37 °C. These data validate
172 our model system and corroborate VACV to be sensitive to thermal restriction at
173 temperatures ≥ 38.5 °C[38]. Analogous infections demonstrated MPXV plaque formation and
174 plaque size to be highly sensitive to alterations in incubation temperature, with reduced
175 numbers of plaques observed at 33 °C, reduced plaque size at 38.5 °C, and a complete
176 inhibition in viral plaque formation at 40 °C (Fig 3F to H). Significantly lower titres of CRV
177 were also detected at 33, 38.5, and 40 °C relative to incubation at 37 °C independently of a
178 block to virus entry (Fig 3I, J). To establish whether the temperature-dependent restriction
179 observed in OPXV replication was a consequence of a failure of HFt cells to support DNA
180 virus replication, we examined the plaque formation of herpes simplex virus 1 (HSV-1, strain
181 17syn+) over an equivalent temperature range. Only a modest restriction in plaque count was
182 observed at 40 °C (Fig S2C), demonstrating HFt cells to support viral DNA replication over a
183 wide range of incubation temperatures. Thus, we identify a low-passage MPXV clinical
184 isolate to be highly sensitive to thermal restriction at both physiological (33 °C) and febrile
185 (38.5 or 40 °C) temperatures relative to incubation at core body temperature (37 °C).
186 As MPXV is known to infect a wide variety of cell types *in vivo*[30], we investigated if
187 the thermal sensitivity of either VACV or MPXV occurred in a cell-type dependent manner.
188 Infection of human normal oral keratinocytes (NOK) and retinal pigmented epithelial (RPE)
189 cells with VACV demonstrated an equivalent trend in thermal restriction to that observed in
190 HFt cells (Fig 4A, B; Fig S2D). Notably, infection of *Chlorocebus sabaeus* or *Chlorocebus*
191 *aethiops* (African green monkey) kidney-derived epithelial or fibroblast cells (Vero E6 and
192 CV-1 cells, respectively) demonstrated significantly higher levels of VACV plaque formation
193 at 33 °C relative to incubation at 37 °C (Fig 4A, B; Fig S2D). These data demonstrate that the
194 thermal permissivity of cells to support VACV replication to be cell-type dependent.
195 Analogous infection with MPXV demonstrated distinct cell-type dependent profiles of
196 thermal restriction at 33 °C (HFt, RPE, and CV-1 cells) and 38.5 °C (NOK, Vero E6, and
197 CV-1 cells) relative to incubation at 37 °C (Fig 4C, D; Fig S2E). All cell lines demonstrated a
198 complete, or near complete (CV-1 cells), restriction in MPXV plaque formation at 40 °C (Fig

199 4C, D). We conclude the basal and ceiling temperatures that support or restrict MPXV
200 replication to be cell-type dependent and distinct from laboratory-adapted VACV.
201
202 **Basal host-cell temperature differentially regulates the outcome of MPXV transcription.**
203 To determine where the block in MPXV replication might occur, we performed RNA
204 sequencing (RNA-Seq) on mock-treated or MPXV-infected HFt cells incubated at 33, 37,
205 38.5 or 40 °C (MOI 0.01 PFU/cell, 48 h). Transcriptome analysis of 28 reference genes
206 known to be expressed across a wide range of tissues and cell-types[41-43] demonstrated no
207 significant difference in their relative profile of expression in mock treated cells across the
208 temperature range of analysis (Fig S3A). Moreover, no significant difference was observed in
209 the total number of host mapped read (MR) counts derived from mock treated samples across
210 the temperature range (Fig S3B, grey bars). These data indicate host-cell transcription to
211 remain largely unperturbed in mock-treated cells up to 40 °C. In contrast, a significant
212 difference in host MR counts was observed in MPXV-infected cells incubated at 33, 37, and
213 38.5 °C relative to mock treatment at 37 °C (Fig S3B, green bars). No significant difference
214 in host MR count was observed between MPXV-infected cells incubated at 40 °C and mock
215 treatment at 37 °C. These data indicate MPXV infection to significantly influence the
216 outcome of host transcription at incubation temperatures permissive to MPXV replication
217 (Fig 3F to I). Investigating further, principal component analysis (PCA) of 178 MPXV ORFs
218 identified significant variance in viral transcript expression (counts per million; CPM) levels
219 at both physiological (33 °C) and febrile (38.5 and 40 °C) temperatures relative to incubation
220 at core body temperature (37 °C) (Fig 5A; Fig S3C). Expression profile analysis identified
221 infected cells incubated at 40 °C to have significantly lower levels of MPXV transcription
222 relative to all other incubation temperatures (Fig 5B, C; Fig S3C). Notably, the overall profile
223 of transcription remained proportionate to that observed at 37 °C, with an approximate 100-
224 fold reduction in transcript expression per ORF at 40 °C (Fig 5B, C). 29 ORFs were
225 identified to have counts below one CPM (Fig 5B, purple circles and text). Of these, 10 ORFs
226 encode proteins involved in intracellular virus maturation, two ORFs that encode virus toll-
227 like receptor (vTLR) antagonists, and three ORFs that encode subunits of the viral RNA
228 (vRNA) polymerase complex (Fig 5D, purple text). Thus, we attribute the ablation of MPXV
229 replication at 40 °C to suppressed levels of viral transcription that bottleneck or restrict the
230 progress of infection. As we had also observed differences in MPXV transcription at lower
231 incubation temperatures (Fig 5A), we next compared the transcription profiles from MPXV

232 infected cells incubated at 33 and 38.5 °C. Relative to 37 °C (Fig 5E, solid grey line), distinct
233 profiles of MPXV transcription could be observed between these two incubation
234 temperatures. Notably, many ORFs displayed opposing profiles of transcription expression
235 (Fig 5E, dotted grey ellipses). Five functionally unrelated ORFs were identified to be
236 downregulated at 33 °C (≥ 1.5 log2 FC) relative to incubation at 37 °C (Fig 5E, orange
237 circles and text). We conclude host-cell temperature to play a key determinant in the
238 differential regulation of MPXV transcription at both physiological skin (33 °C) and febrile
239 (38.5 or 40 °C) temperatures relative to core body temperature (37 °C). Collectively (Figs 2
240 to 5), these data identify the optimal temperature for MPXV Clade IIb.B1 replication to be 37
241 °C.
242
243 **Basal temperature differentially regulates the host-cell response to MPXV infection.**
244 As we had identified temperature to differentially regulate MPXV transcription (Fig 5), we
245 next investigated the influence of temperature on the host-cell response to infection. We
246 performed RNA-Seq analysis on mock-treated or MPXV-infected HFt cells incubated at 33,
247 37, 38.5 or 40 °C (MOI 0.01 PFU/cell, 48 h). Pairwise comparisons identified unique and
248 shared clusters of DEGs (FDR < 0.05, ≥ 1.5 log2 FC) across the temperature range of
249 analysis (Fig 6A, B). Relatively few DEGs were identified between mock-treated and
250 infected samples incubated at 40 °C, suggesting MPXV infection at this temperature to
251 induce a minimal host-cell response (Fig 6A, B; yellow ellipses and lines). This was
252 surprising, as we had observed equal levels of MPXV genome entry into infected cells across
253 the temperature range of analysis (Fig 3J). These data identify the onset of MPXV replication
254 to be a key determinant in the host-cell response to infection. Pathway analysis identified
255 distinct profiles of DEG enrichment dependent on incubation temperature, with 33 and 38.5
256 °C sharing the highest degree of similarity in their respective host-cell responses to infection
257 (Fig 6C, grey lines). Notably, many pathways were only significantly enriched in response to
258 infection at 37 °C (Fig 6C), even though cells incubated at 33 and 38.5 °C were observed to
259 be productively infected and to be releasing infectious virus (Figs 2 to 4). These data
260 demonstrate basal host-cell temperature to play a key role in the outcome and/or amplitude of
261 host-cell response to MPXV infection. Consistent with this finding, we observed multiple
262 cytokine-related pathways to be differentially regulated in response to MPXV infection (Fig
263 6C, black arrows). Analysis of these DEGs (71 genes in total) revealed distinct profiles of
264 immune gene expression that were dependent on both infection and incubation temperature

265 (Fig 6D to F). Importantly, this host-cell immune signature to infection occurred
266 independently of the robust induction of the type-I IFN response (Fig 6G; Fig S4A, B). While
267 *IFNB1* was identified to be a DEG (Fig 6G, black arrow), levels of *IFNB1* expression were
268 extremely low (MPXV 37 °C mean CPM = 0.1285, -/+ 0.02 SD; Fig S4A, B), with little to
269 no change observed in the overall profile of host interferon responsive genes (IRGs; Fig S4C,
270 D). These data demonstrate Clade IIb.B1 MPXV infection to effectively suppress the
271 induction of IFN-mediated antiviral immune defences. Notably, MPXV-infected cells
272 incubated at 40 °C expressed an equivalent cytokine profile to that of mock treatment at this
273 incubation temperature (Fig 6D, E [purple arrow]; Fig S4E). Thus, viral genome entry into
274 host-cells alone is not sufficient to trigger the activation of pathogen recognition receptors
275 (PRRs) necessary for the induction of cytokine-mediated pro-inflammatory immune
276 responses to infection. Collectively, these data demonstrate MPXV to induce a temperature-
277 dependent cytokine response to infection dependent on the productive onset of viral lytic
278 replication (Fig 3F to I).
279 Investigating further, we compared the host-cell transcriptome profiles of MPXV
280 infected cells incubated at 37 and 40 °C. Out of the 935 DEGs (FDR <0.05, ≥ 1.5 log2 FC)
281 identified (Fig 7A), pathway analysis identified cell cycle (Fig 7B, grey arrow and circle) and
282 immune system (Fig 7B, coloured arrows and circles) related pathways to be predominantly
283 downregulated at 40 °C relative to incubation at 37 °C (Fig 7B). Analysis of immune system
284 related DEGs (61 genes in total) identified signalling by interleukin (IL; 20 DEGs) and
285 adaptive immune system (21 DEGs) pathways to account for the majority of DEGs identified
286 between these two infection conditions (Fig 7C, D). In contrast to IFN signalling (Fig S4A to
287 D), analysis of the IL signalling pathway (R-HAS-449147; 459 genes in total) identified this
288 pathway to be significantly upregulated during MPXV infection in a temperature-dependent
289 manner (Fig 7D green dots; Fig S4F). Notably, multiple cytokines and chemokines
290 implicated in IL signalling were observed to vary in their relative profiles of expression
291 between 33 and 38.5 °C (Fig 7E; e.g., IL12A [P = 0.0026], CXCL2 [P = 0.0013]).
292 Importantly, MPXV incubation at 40 °C failed to upregulate these cytokine-related genes
293 above baseline levels (Fig 7D, E; Fig S4E, F). Together, these data demonstrate MPXV to
294 induce a robust IL response to infection in a temperature-dependent manner.
295

296 **Basal temperature differentially regulates the host-cell IFN response to MPXV**
297 **infection.**
298 As the IFN response is known to play a key role in limiting OPXV pathogenicity and
299 immune clearance *in vivo*[44,45], we next investigated whether basal host-cell temperature
300 influenced the IFN-mediated host-cell restriction of MPXV. HFt cells were stimulated with
301 IFN-β and incubated at 33, 37, 38.5 or 40 °C for 16 h prior to MPXV infection (MOI 0.001
302 PFU/cell) and continued incubation in the presence of IFN for 48 h at their respective
303 temperatures. Quantitation of plaque counts demonstrated MPXV restriction to occur in an
304 IFN-β dose- and temperature-dependent manner, with heightened levels of restriction
305 observed at 38.5 °C relative to incubation at 33 or 37 °C (Fig 8A to D). Consistent with our
306 previous analysis (Figs 2 to 4), MPXV plaque formation was abrogated at 40 °C irrespective
307 of IFN stimulation (Fig 8A, B grey dotted lines and circles). IFN pre-treatment and infection
308 with VACV demonstrated an analogous dose- and temperature-dependent trend in VACV
309 restriction that abrogated plaque formation at 40 °C in the presence of 100 IU/ml of IFN-β
310 (Fig S5A to D). As temperature elevation alone led to suppressed levels of MPXV
311 transcription independently of the robust induction of the type-I IFN response (Figs 5, 6, S4A
312 to D), we next investigated the synergistic nature of temperature elevation and IFN co-
313 stimulation on the outcome of MPXV infection. Naïve HFt cells were infected with MPXV
314 (MOI 0.01 PFU/cell) for 1 h at 37 °C prior to stimulation with IFN-β and incubation at 33,
315 37, 38.5 or 40 °C. Infected and treated cell monolayers were fixed at 24 hpi and the number
316 of MPXV virion antigen positive cells quantified by immunostaining. Consistent with our
317 IHC analysis of infected tissues (Fig 2), incubation temperature dramatically reduced the
318 number of MPXV virion antigen positive cells detected at 24 hpi (Fig 8E, F; 0 IU/ml IFN-β,
319 37°C > 33 ≈ 38.5 °C > 40 °C). Notably, a substantial number of MPXV antigen positive cells
320 could still be detected at 40 °C, indicating that a proportion of MPXV genomes were able to
321 circumvent complete thermal restriction (Fig 8E, F; 0 IU/ml IFN). Co-stimulation with IFN-
322 β led to a dose- and temperature-dependent reduction in the number of antigen positive cells
323 (Fig 8E, F plus IFN). These data identify temperature elevation to cooperate and synergise
324 with the type-I IFN response to mediate the host-cell restriction of MPXV. As neither
325 temperature elevation nor IFN stimulation was sufficient to eliminate MPXV gene expression
326 (Fig 8E, F), we hypothesised MPXV replication may recover following temperature
327 downshift to 37 °C and/or withdrawal of IFN as an immune stimulus. Downshift of infected
328 cells from 40 (no IFN treatment) to 37 °C led to a complete recovery in MPXV plaque

329 formation to equivalent levels observed at 37 °C (Fig 8G). These data demonstrate MPXV
330 thermal restriction to only stall the progress of infection, as opposed to eliminate or induce
331 the establishment of viral genome quiescence. Surprisingly, IFN washout from infected and
332 IFN-treated cells incubated at 37 °C also led to an equivalent recovery (Fig 8H). Analogous
333 to temperature restriction, these data demonstrate the type-I IFN response to suppress, but not
334 eliminate, MPXV infection. Importantly, IFN washout and thermal downshift of MPXV-
335 infected and IFN-stimulated cells from 40 to 37 °C led to significantly lower recovery in the
336 re-establishment of MPXV infection in an IFN dose-dependent manner (Fig 8J). Equivalent
337 trends in the re-establishment of infection were also observed following IFN washout and
338 temperature downshift of VACV infected cells (Fig S5G to J). We conclude temperature
339 elevation to synergise with and enhance the type-I IFN-mediated restriction of MPXV to
340 limit the re-establishment of infection upon homeostatic recovery from these two independent
341 pro-inflammatory immune responses known to be activated in response to infection *in*
342 *vivo*[32,46].
343

344 **Discussion**

345 The emergence of novel MPXV Clade IIb variant strains that support heightened levels of
346 human-to-human transmission is a global health concern and highlights the need for a better
347 understanding of MPXV and its interaction with the host immune system. The pro-
348 inflammatory fever response is a well-established and common prodrome symptom of
349 MPXV infection[11,14-17], but the precise thermoregulatory impact on the outcome of infection
350 has remained poorly defined. Here, we isolated a clinical Clade IIb.B.1 MPXV strain (MPXV
351 CVR_S1) from a hospitalised patient admitted with fever (38.5 °C) to determine the
352 influence of temperature elevation on the outcome of MPXV infection.
353 Previous studies (circa 1960s) have shown OPXVs to have divergent ceiling
354 temperatures of pox formation in the chorioallantoic membrane of infected embryonic
355 chicken eggs, ranging from 38 °C to ≥ 40.5 °C (VARV minor to VACV, respectively)[33,34].
356 Here we show the clinical febrile temperature range of 38.5 to 40 °C, representative of low-
357 to moderate-grade fever in humans[11,14-17,21], to restrict the replication of a circulating MPXV
358 Clade IIb strain. This temperature-dependent restriction was observed across a variety of
359 infection models (Figs 2 to 4), including pseudostratified skin epithelium, and is consistent
360 with the reported ceiling temperature of MPXV pox formation in embryonic chicken eggs of
361 39.5 °C[33]. Collectively, these data demonstrate that febrile temperatures associated with

362 mpox disease in humans are likely to be a key determinant in the outcome of infection.
363 Importantly, we show that the thermal restriction of MPXV to occur independently of a block
364 to virus entry (Fig 3J) and to be reversible upon temperature downshift without impairment to
365 viral replication fitness (Fig 8G). These findings are consistent with the re-establishment of
366 VARV replication in embryonic chicken eggs upon thermal downshift from its inhibitory
367 ceiling temperature of 38.5 °C[34]. As OPXVs with alternate ceiling temperatures have been
368 shown to complement quiescent infections leading to hybrid pox formation[34,47], variance in
369 MPXV Clade and strain ceiling temperatures might contribute to genetic reassortment during
370 mixed co-infection and/or changes in viral pathogenesis. Thus, the thermoregulatory
371 mechanisms surrounding MPXV genome stability, longevity, and retention of replication
372 fitness at febrile temperatures warrants further investigation. Importantly, we demonstrate
373 lower physiological temperatures associated with skin tropism to also impact on MPXV
374 replication. We observed a significant reduction in MPXV intraepithelial propagation, plaque
375 formation, and virus yield following incubation at 33 °C (Figs 2 to 4). We posit the fever
376 response to both positively and negatively influence the outcome of OPXV infection
377 dependent on the baseline temperature of the tissue at the point of infection. For example, a
378 general two to four °C rise in skin temperature from 33 to 37 °C would be expected to
379 promote MPXV replication, whereas a similar rise in tissue temperature from 37 °C we show
380 to be progressively inhibitory (Figs 2 to 4). Thus, inherent differences in species body/tissue
381 temperature and/or capacity to mount a febrile immune response could impact on the
382 zoonotic potential of MPXV to be maintained within an animal reservoir or to undergo inter-
383 species host transmission. Indeed, available evidence suggests small rodent models to have
384 variable febrile responses to OPXV infection, potentially in an MPXV Clade dependent
385 manner[22,30-32]. Thus, the influence of tissue temperature on MPXV species tropism and
386 onward transmission also warrants additional investigation.
387 Our transcriptomic analysis demonstrates host-cell temperature to have a significant
388 impact on the differential regulation of viral transcription and associated host-cell responses
389 to MPXV infection, both at physiological (33 °C) and febrile (38.5 and 40 °C) temperatures
390 relative to core body temperature (37 °C; Figs 5 to 7). MPXV incubation at 40 °C led to a
391 substantial decrease in viral transcription (≈ 100-fold reduction per ORF; Fig 5B, C).
392 However, the overall profile of transcription remained proportionate to that observed at 37 °C
393 (Fig 5B), indicative of a genome-wide suppression in transcription, as opposed to a specific
394 block in the expression of any individual viral ORF. Notably, we identify multiple viral

395 ORFs that encode proteins associated with virion maturation to show substantially decreased
396 transcript levels (< 1 CPM per ORF; Fig 5B, D). Consistent with this observation,
397 significantly lower levels of virion antigen expression were also observed within MPXV-
398 infected tissues or cells incubated at 40 °C (Figs 2, 8E). Thus, temperature elevation is likely
399 to cause a bottleneck in the expression of critical viral gene products required for virion
400 maturation that suppress the onward propagation and spread of MPXV. Notably, differential
401 patterns of MPXV transcription and replication fitness were also observed at lower
402 temperatures (Figs 2, 3, 4, 5E). Incubation at 33 °C led to a 50 % decrease in viral plaque
403 formation, whereas incubation at 38.5 °C resulted in a 50 % decrease in viral plaque size
404 relative to incubation at 37 °C (Figs 3G, H, 4C). Together, these data highlight the
405 importance of basal host-cell temperature to the outcome of MPXV infection. We posit that
406 the differential patterns of viral transcription observed between 33 and 38.5 °C to account for
407 the phenotypic differences identified between these two incubation temperatures. Of the five
408 viral ORFs identified to be significantly downregulated at 33 °C (Fig 5E, orange circles),
409 experimental evidence has shown the VACV orthologues of gp148 (VACV A43R), gp007
410 (VACV D6L), and gp146 (VACV A41L) to impact on viral replication fitness and lesion
411 formation[48-51]. Thus, the differential patterns of viral transcription observed at both
412 physiological and febrile temperatures are likely to affect multiple viral and cellular
413 processes that govern the overall outcome of infection.
414 Our host-cell transcriptome analysis of mock-treated or MPXV-infected cells
415 incubated at 40 °C identified relatively few DEGs at this incubation temperature (13 in total;
416 Fig 6A, B). This minimal host-cell response correlates with the limited levels of MPXV
417 transcription and replication observed at 40 °C (Figs 2 to 5). Thus, viral genome entry into
418 host-cells alone is not sufficient to activate PRRs sufficient to induce a robust pro-
419 inflammatory immune response to infection (Figs 6, S4). In contrast, we identify a significant
420 induction of pro-inflammatory interleukin gene expression at both physiological skin, core,
421 and febrile temperatures (33, 37 and 38.5 °C, respectively) permissive to MPXV replication.
422 These differential patterns of interleukin and chemokine expression correlate well with the
423 levels of MPXV replication observed at these incubation temperatures. For example, IL-6
424 induction (a key pyrogen in the regulation of the fever response[52]) demonstrated peak
425 induction at 37 °C, with lower levels of induction observed at 33 or 38.5 °C (Fig 7E),
426 consistent with decreased levels of replication observed at these incubation temperatures
427 (Figs 2, 3). Thus, we identify basal host-cell temperature to be a key determinant in the
428 amplitude of cytokine response to MPXV infection. These data are consistent with cytokine

429 profiling experiments of serum samples derived from experimentally infected NHPs or
430 hospitalised patients that have shown pro-inflammatory interleukin expression levels to
431 correlate with the kinetics of MPXV replication and disease severity, respectively[32,46]. While
432 MPXV encodes immune antagonists to IL-1 (gp014, gp152, gp167), IL-18 (gp007), TNF-α
433 (gp002, gp178), IFN-α/β (gp169), and IFN-γ (gp163), among others[44], it does not encode a
434 direct IL-6 antagonist. This raises the possibility that specific profiles of pro-inflammatory
435 cytokine or chemokine expression may be beneficial to MPXV replication prior to
436 temperature elevation, potentially through the recruitment and infection of bystander and/or
437 circulating immune cells to promote virus dissemination[44].
438 The type-I IFN response is a critical component of the host's antiviral immune
439 defence, which acts to restrict viral propagation and to prime adaptive immune responses to
440 clear MPXV infection[44,45,53-55]. Due to their large coding capacity, OPXVs encode multiple
441 immune antagonists to block the induction of the type-I IFN response at several independent
442 stages of infection[44,45,56,57]. Correspondingly, we demonstrate a clinical and circulating
443 MPXV IIb.B1 strain to effectively suppress the induction of the type-I IFN response (Figs 6,
444 S4). Importantly, the activation of PRRs that regulate the pro-inflammatory IFN response can
445 be triggered through multiple mechanisms, including the detection of damage-associated
446 molecular patterns (DAMPs) in addition to pathogen associate molecular patterns (PAMPs).
447 We posit the IFN signature observed in response to MPXV infection *in vivo* is likely a
448 consequence of DAMP activation due to the high levels of replication observed in multiple
449 cell-types and organs upon viral dissemination[32,44,46]. We demonstrate a circulating clinical
450 MPXV IIb.B.1 strain to be sensitive to exogenous IFN-β stimulation in a dose- and
451 temperature-dependent manner (Fig 8). These data are consistent with previous reports that
452 have shown Clade I MPXV strains to be sensitive to exogenous IFN stimulation at 37 °C[53,55].
453 Importantly, we demonstrate this IFN-mediated restriction to be reversible and not to
454 effectively eliminate infection, with significantly lower levels of MPXV recovery observed at
455 febrile temperatures associated with clinical infection (Fig 8H, J). Thus, we identify
456 functional cooperativity and synergism between pro-inflammatory immune responses (fever
457 plus IFN) that mediate the accumulative host-cell restriction of MPXV. Such accumulative
458 effects are likely to be a consequence of suppressed levels of viral transcription at febrile
459 temperatures restricting the ability of MPXV to express immune antagonists that directly
460 counteract the effects of IFN (e.g., the viral IFN-α/β receptor antagonist gp169)[56]. We posit
461 that such synergism between pro-inflammatory immune responses will likely play a

462 significant role *in vivo* to limit MPXV propagation and to prime adaptive immune responses
463 required for immune clearance[54].
464 In conclusion, our study provides critical insights into the importance of temperature
465 in the regulation and outcome of MPXV infection. We identify host-cell temperature at both
466 physiological and febrile temperatures to be a key determinant in the regulation of viral
467 transcription, associated amplitude of cytokine response to infection, and ancillary
468 interactions with the type-I IFN response required to inhibit MPXV replication. Our data
469 shed light on the complex interplay and functional synergy between host pro-inflammatory
470 immune systems and their net combinatorial affect on the outcome of OPXV infection,
471 findings pertinent to the immune regulation of many clinical pathogens that induce a fever
472 response.
473

474 ## Materials and Methods

475 **Cells and cell viability assays**

476 Vero E6 (a gift from Michelle Bouloy, Institute Pasteur, France), CV-1 (European Collection
477 of Authenticated Cell Cultures (EACC), 87032605), HFt[58], RPE-1 (ATCC, CRL-4000),
478 HaCaT (Addexbio, T0020001), and J2 3T3 (a gift from Sheila Graham, MRC-University of
479 Glasgow Centre for Virus Research) cells were grown in Dulbecco's Modified Eagle
480 Medium (DMEM; ThermoFisher, 10566016) supplemented with 10 % fetal bovine serum
481 (FBS; ThermoFisher 10270106) and 1 % penicillin streptomycin (PS; ThermoFisher,
482 15070063). NOK cells (a gift from Karl Munger, Tufts University School of Medicine,
483 USA)[59] were grown in Keratinocyte-SFM medium with L-glutamine, EGF, and BPE
484 (ThermoFisher, 17005075). All cells were grown and maintained at 37 °C in 5 % CO_2 unless
485 otherwise stated. Cell viability was measured using MTS reagent (Abcam, ab197010), as per
486 the manufacturer's guidelines, and absorbance measurements taken at OD=490 nm using a
487 PHERAstar plate reader (BMG LABTECH). As a positive control for cell death, puromycin
488 (Sigma-Aldrich, P8833) was added to cell culture media at a final concentration of 1.0 □g/ml
489 and incubated for 24 h prior to the addition of MTS.
490

491 **Organotypic raft culture**

492 Type I collagen was extracted from rat tails (supplied by the University of Glasgow,
493 Veterinary Research Facility). Ethanol sterilised tails were incubated in 0.5 M acetic acid at 4
494 °C for 48 hours on a magnetic stirrer. Material was clarified by centrifugation at 10,000 x g

495 for 30 minutes at 4 °C. Supernatant was subjected to collagen extraction by NaCl
496 precipitation (final concentration 10 % weight/volume) for 1 h at 4 °C and collected by
497 centrifugation at 10,000 x g for 30 minutes at 4 °C. The pellet was resuspended overnight in
498 0.25 M acetic acid and dialysis for three days (two changes per day) in pre-cooled acetic acid
499 (final concentration 17.4 mM) at 4 °C. Sterile collagen was isolated by centrifugation 20,000
500 x g for 2 h at 4 °C. Organotypic raft cultures were prepared as previously described[60]. Briefly,
501 collagen matrices with J2 3T3 fibroblasts were prepared in 12-well plates and allowed to
502 contract for approximately 7 days at 37 °C. Keratinocytes (HaCaT cells) were seeded on top
503 of contracted collagen matrices at a density of $2.5x10^5$ cells/matrix in 24-well plates and
504 incubated at 37 °C overnight prior to being transferred into Costar Transwells (Corning
505 Costar, 3401) and maintained at 37°C under air liquid interface (ALI) for 12 to 14 days.
506 Tissues were maintained in E-medium (3:1 ratio of DMEM:F12 (Thermofisher, 21765029)
507 medium supplemented with 10 % FBS and 1 % PS, 2 mM L-glutamine (ThermoFisher,
508 25030081), 180 µM adenine (Sigma-Aldrich, A2786), 5 µg/ml transferrin (Sigma-Aldrich,
509 T1147), 5 µg/ml insulin (Sigma-Aldrich, I6634), 0.4 mg/ml hydrocortisone (Sigma-Aldrich,
510 H0888), 0.1 nM cholera toxin (Sigma-Aldrich, C8052), and 0.2 ng/ml epidermal growth
511 factor (EGF; Sigma-Aldrich, E9644). Basal-chamber E medium was changed every 48 h.
512 Pseudostratified skin tissues were infected with 10^2 or 10^3 pfu/tissue (as indicated) in 50 µl
513 inoculum for 1 h at 37 °C prior to incubation at the indicated temperatures for 72 h.
514
515 **Immunohistochemistry**
516 Mock treated or infected pseudostratified skin epithelia was fixed in 8% (v/v) formaldehyde
517 overnight, washed in PBS, and processed by the Diagnostic Services, School of Biodiversity,
518 One Health and Veterinary Medicine, University of Glasgow. Following paraffin embedding,
519 3 µm sections were cut and placed in a 37 °C oven overnight. Samples were dewaxed in
520 HistoClear (National Diagnostics, HS-20) and rehydrated through 3x sequential washes in
521 ethanol (final concentration 70 %). Tissue sections were subject to antigen retrieval using
522 TET buffer (10 mM Tris base pH 9, 1 mM EDTA, 0.05% Tween-20) in a MenaPath access
523 retrieval unit at 125 °C and 15 psi for 100 sec, before cooling to room temp in H_2O and
524 transfer to TNET buffer (10 mM Tris pH 7.5, 100 mM NaCl, 1 mM EDTA, 0.05 % Tween-
525 20). Tissue sections were stained with a polyclonal antibody raised against whole VACV
526 (Invitrogen, PA1-7258; 1/2000 dilution) for 30 mins, washed in TNET buffer, prior to
527 secondary staining (Dako Envision polymer anti-rabbit, K4003) for 30 mins and washing in
528 TNET buffer. Visualisation was achieved using two 5 min applications of DAB+ (Dako,

529 K3468). Tissue sections were counterstained using Gills haematoxylin dehydrated, prior to
530 clearing in Histoclear, and mounting with a coverslip. Tissue sections were imaged using an
531 Aperio VERSA Digital Pathology Scanner (Leica Biosystem). Scanned tissue sections were
532 quantified using the Halo multiplex IHC module image analysis software (indica labs). The
533 algorithm was adapted for nuclei identification and arbitrary thresholds applied to detect
534 weak, moderate, and strong MPXV antigen positive cells over background levels of staining.
535 Algorithm optimisation was performed using the real-time Tuning function. All sections were
536 analysed using the same algorithm and subjected to random checks to confirm the precision
537 of tissue annotation.
538
539 **Viruses**
540 Clinical monkeypox virus (MPXV) CVR_S1 was isolated from an ISARIC4C patient with
541 ethical consent (Ethics approval for the ISARIC CCP-UK study was given by the South
542 Central–Oxford C Research Ethics Committee in England (13/SC/0149), the Scotland A
543 Research Ethics Committee (20/SS/0028) and the WHO Ethics Review Committee (RPC571
544 and RPC572). The patient presented with fever (38.5 °C), cough, myalgia, and skin rash. The
545 patient was haemodynamically stable and not requiring supplemental oxygen. Swabs were
546 collected from multiple skin lesions into virus transport medium (VTM). The VTM was
547 mixed in a 1:4 ratio with DMEM supplemented with 10 % FBS, 1 % PS and 250 ng/ml
548 Amphotericin B (ThermoFisher, 15290018) and centrifuged at 4000 rpm for 10 mins. Vero
549 E6 (sub-clone MESO; a gift from Meredith Stewart, MRC - University of Glasgow Centre
550 for Virus Research) cells were inoculated with 500 □l of VTM/media for 1 h. Infected
551 monolayers were washed three times in PBS prior to overlay with cell culture media and
552 incubation at 37 °C in the presence of 5 % CO_2. Media containing infectious cell-released
553 virus (CRV; primary amplification P1 stock) was harvested at 72 hours post-infection (hpi)
554 and clarified at 4000 rpm for 10 minutes. P1 virus was subjected to Illumina metagenomic
555 sequencing to evaluate purity and sequence homology to pre-culture clinical material
556 (CVR_MPXV1a; accession number ON808413) to confirm sequence identity and source of
557 the propagated isolate. All experiments were performed in a Biosafety level 3-laboratory at
558 the MRC-University of Glasgow Centre for Virus Research (SAPO/223/2017/1a). Vaccinia
559 Virus (VACV A5L-EGFP, a gift from Geoffrey Smith, University of Oxford, England)[61] was
560 propagated and titrated on Vero E6 (MESO) cells, as previously described[61,62]. Wild-type
561 herpes simplex virus 1 (HSV-1, strain 17syn+; a gift from Roger Everett, MRC - University

562 of Glasgow Centre for Virus Research) was propagated in RPE cells and titred on U2OS
563 cells, as previously described[63].
564
565 **Viral genome sequencing**
566 20 ng of nucleic acid was enriched for viral genomic sequences using NEBNext Microbiome
567 DNA Enrichment Kit (NEB, E2612) to reduce host genomic DNA contamination. Purified
568 DNA was sheared into 350-base pair fragments by sonication using the Covaris Sonicator
569 LE220. Library preparation was conducted with the KAPA Hyper kit (Roche, 07962347001)
570 with end repair and universal adapter ligation. Unique Dual Index Primer pairs (NEBNext
571 Multiplex Oligos for Illumina) were used to index the samples, followed by 10 cycles of PCR
572 amplification. Libraries were sequenced on the Illumina NextSeq500 platform with paired
573 ends for 2 x 150-base pair reads using a Mid-output cartridge Kit v2.5 (Illumina,
574 20024905). bcl2fastq software was used to demultiplex and compress bcl files into fastq (gz)
575 files. Short and low-quality sequence reads (length < 75 nucleotides, Phred score < 30) were
576 filtered from the fastq files using Trim Galore (version 0.6.6). BWA-MEM (version 0.7.17-
577 r1188) was used to map filtered reads to the reference sequence. Ivar (version 1.3.1) program
578 generated consensus sequences (minimum depth 10 reads and consensus frequency threshold
579 0.6) from the aligned BAM files. Consensus sequences were manually checked, and repeat
580 regions were curated based on majority read consensus. Multiple sequence alignment was
581 performed using MAFFT (v7.475)[64] and aligned to the MPXV Clade IIa reference sequence
582 (NC_063383.1). Variations between the sequences were plotted using the Snipit program
583 (v.1.1.2). APOBEC3-associated mutations (G=>A and C=>T) were calculated from pairwise
584 sequence alignment using a BASH script.
585
586 **Plaque and virus yield assays**
587 Cells were seeded onto plates and allowed to become confluent before infection at the
588 specified multiplicity of infection (MOI) for 1 h at 37 °C prior to overlay and incubation at
589 the indicated temperatures. For infectious cell-released virus (CRV) quantitation, harvested
590 supernatants were serially diluted in cell culture media and used as an inoculum to infect
591 Vero E6 (MESO) cells to obtain a linear range of countable plaques. Infected monolayers
592 were incubated at 37 °C for 24 to 72 h (dependent on the virus and experiment), fixed with 4
593 (VACV) or 8 (MPXV) % (v/v) formaldehyde (Sigma-Aldrich, F8775), washed in PBS, and
594 stained with 0.1 % Coomassie Brilliant Blue solution (Sigma-Aldrich, B0149) in 45 %

595 methanol and 10 % acetic acid for up to 30 minutes. Plates were washed in water and dried
596 overnight before plaque counting under a plate microscope. For quantitation of plaque
597 diameters, infected cell monolayers stained with Coomassie Brilliant Blue were imaged using
598 a Celigo Imaging Cytometer (Nexcelom Bioscience, UK) and plaque measurements
599 performed using Zen Blue software (Zeiss).
600

601 **Temperature and Interferon (IFN) inhibition assays**

602 Cells were infected at 37 °C for 1 h at the indicated MOI prior to overlay and continued
603 incubation at the desired temperature (33, 37, 38.5, or 40 °C) in 5 % CO_2 for the indicated
604 times prior to fixation and Coomassie Brilliant Blue or indirect immunofluorescence staining.
605 For IFN inhibition assays, cell monolayers were either pre-treated with IFN-β (R&D systems,
606 8499-IF-010; 0.1 to 200 IU/ml, as indicated) for 16 h at the indicated temperatures prior to
607 infection or infected for 1 h at 37 °C prior to the addition of IFN-β to the overlay and
608 incubation at the desired temperature (as indicated). For temperature downshift and IFN
609 washout experiments, duplicate infected plates were overlayed with media containing IFN-β
610 (0 to 200 IU/ml; as indicated) for 24 or 48 h (VACV or MPXV, respectively) prior to either
611 fixation or IFN washout (3x 1 ml cell culture media) and continued incubation at 37 °C for
612 24 or 48 h prior to fixation and Coomassie staining.
613

614 **Indirect immunofluorescence**

615 Mock treated, infected, or infected and IFN treated cells were fixed with 4 (VACV) or 8
616 (MPXV) % (v/v) formaldehyde, washed in PBS, and permeabilised with 0.5 % Triton-X-100
617 (Sigma-Aldrich, T-9284) prior to blocking in filter sterilised PBS containing 2 % FBS
618 (PBSf). Cells were stained with a polyclonal antibody raised against whole VACV
619 (Invitrogen, PA1-7258; 1/2000 dilution) and secondary staining using a donkey anti-rabbit
620 AlexaFluor 555 (Invitrogen, A31572). Cell nuclei were stained with DAPI (Sigma-Aldrich,
621 D9542). PBSf was used for all antibody incubations (1 h at RT) and cell washing throughout.
622 Cell monolayers were imaged and analysed using a Celigo Imaging Cytometer and
623 companion software (Nexcelom Bioscience, UK).
624

625 **Quantitative PCR (qPCR)**

626 PCR was carried out using NEB Luna Universal Probe One-Step RT-qPCR Kit (New
627 England Biolabs, E3006) or Taqman Fast Universal PCR master mix (Applied Biosystems,

628 4352042), according to the manufactures' instructions. VACV was detected using primers
629 and probe directed to ORF E9L[65]; E9L forward primer: 5'-
630 CGGCTAAGAGTTGCACATCCA-3', E9L reverse primer: 5'-
631 CTCTGCTCCATTTAGTACCGATTCT-3' and E9L Probe 5'-
632 [6FAM]AGGACGTAGAATGATCTTGTA[BHQ1]-3'. MPXV was detected using the
633 primers and probe directed against the ORF G2R[66]; G2R FWD: 5'-
634 GGAAAATGTAAAGACAACGAATACAG-3', G2R REV 5'-
635 GCTATCACATAATCTGGAAGCGTA-3' and G2R Probe 5'-
636 [6FAM]AAGCCGTAATCTATGTTGTCTATCGTGTCC[BHQ1]-3'. 5 □l of extracted DNA
637 was used per 20 □l reaction and thermal cycling was performed on an Applied Biosystems
638 7500 Fast PCR instrument running SDS software v2.3 (ThermoFisher Scientific) under the
639 following conditions: 95 °C for 5 mins, followed by 45 cycles of 95 °C for 10 s and 62 °C for
640 30 mins.
641
642 **Viral entry assays**
643 HFt cells were seeded in 6-well plates at a cell density of $4x10^5$ cells/well 24 h prior to
644 infection. Cells were infected with MPXV or VACV at a MOI 0.1 PFU/cell for 1 h at 37 °C
645 before continued incubation at the desired temperature (as indicated) for a further 1 h. Cell
646 monolayers were washed twice in PBS before being trypsinised. Cells were pelleted at 3000
647 rpm for 5 mins and resuspended in 200 □l PBS. Total DNA was extracted using QIAamp
648 DNA kit (Qiagen, 51304), according to the manufacturer's instructions, with a final elution
649 volume of 20 □l. Viral genome levels were quantified by qPCR using virus specific primer
650 probe sets (described above) and normalised to GAPDH using an Applied Biosystems
651 FAM/MGB probe mix (Thermofisher, 4333764F).
652
653 **RNA sequencing (RNA-Seq)**
654 HFt cells were seeded onto 12-well plates at a density of $2x10^5$ cells/well. 24 h post-seeding,
655 cells were mock treated or infected with MPXV CVR_S1 (MOI 0.01) for 1h at 37 °C before
656 overlay and continued incubation at 33, 37, 38.5 or 40 °C (as indicated). Cells were washed
657 three times in PBS at 48 h prior to RNA extraction using a RNeasy plus Micro Kit (Qiagen,
658 74034). Eluted RNA was quantified using Qubit Fluorometer 4 (ThermoFisher, Q33238),
659 Qubit RNA HS Assay (Life Technologies, Q32855) and dsDNA HS Assay Kits
660 (ThermoFisher, Q32854) and quality controlled on a 4200 TapeStation System (Agilent
661 Technologies, G2991A) with a High Sensitivity RNA Screen Tape assay (Agilent

662 Technologies, 5067-5579). All samples had a RIN score of ≥ 8.8. 220 ng of total RNA was
663 used to prepare libraries for sequencing using an Illumina TruSeq Stranded mRNA Library
664 Prep kit (Illumina, 20020594) and SuperScript II Reverse Transcriptase (Invitrogen,
665 18064014) according to the manufacturer's instructions. Dual indexed libraries were PCR
666 amplified, purified using AgencourtAMPure XP magnetic beads (Beckman Coulter,
667 10136224), quantified using Qubit Fluorometer 4 (TheroFisher, Q33238) and Qubit dsDNA
668 HS Assay Kit (ThermoFisher, Q32854), and the size distribution assessed using a 4200
669 TapeStation System (Agilent Technologies, G2991A) with a High Sensitivity D1000 Screen
670 Tape assay (Agilent Technologies, 5067-5584). Libraries were pooled in equimolar
671 concentrations and sequenced using an Illumina NextSeq 500/550 sequencer (Illumina, FC-
672 404-2005). At least 95% of the reads generated presented a Q score of ≥ 30. RNA-Seq reads
673 were quality assessed using FastQC
674 (http://www.bioinformatics.babraham.ac.uk/projects/fastqc). Sequence adaptors removed
675 using TrimGalore (https://www.bioinformatics.babraham.ac.uk/projects/trim_galore/). RNA-
676 Seq reads were aligned to the *Homo sapiens* genome (GRCh38), downloaded via Ensembl
677 using HISAT2. HISAT2 is a fast and sensitive splice aware mapper, which aligns RNA
678 sequencing reads to mammalian-sized genomes using FM index strategy[67]. FeatureCounts[68]
679 was used to calculate mapped read counts that were normalized to counts per million (CPM;
680 unless otherwise stated). Generalized linear models (GLMs) with multi-factor designs was
681 used for differential gene expression (DEG) analysis in EdgeR[69]. An FDR (False Discovery
682 Rate) value <0.05 was used as a cut-off of significant differential gene expression. Viral
683 sequences were aligned to the MPXV Clade IIa reference sequence (NC_063383.1). High
684 confidence (FDR <0.05, ≥ 1.5 log2 fold change [FC]) DEGs were used for pathway analysis
685 in Reactome (https://reactome.org)[70,71] or differential pathway analysis in Metascape
686 (https://metascape.org/gp/index.html#/main/step1)[72]. For Reactome analysis, the gene
687 mapping tool was used as a filter to identify pathways enriched (over-represented) for
688 mapped entities. FDR values <0.05 were considered significant for pathway enrichment. In
689 Metascape, all DEGs were used for differential pathway analysis. Pathway *p*-values <0.05
690 were considered significant. Heat maps were plotted in GraphPad Prism (version 10). Mean
691 counts per million (CPM) values of zero were normalized to 0.01 for log2 presentation. Venn
692 diagrams were plotted using http://bioinformatics.psb.ugent.be/webtools/Venn/. RNA-Seq
693 datasets generated from this study have been deposited in the European Nucleotide Archive
694 (ENA), accession number PRJEB66116.
695

696 **Statistical analysis**

697 The number (N) of independent biological experiments is shown throughout. GraphPad
698 Prism (version 10) was used for PCA and statistical analysis. Statistical tests and *p*-values are
699 shown throughout. Statistically significant differences were accepted at $p<0.05$.

700

701 **Data availability**

702 All datasets generated and analysed in this study will be made freely available in
703 supplemental files or online (ENA; accession number PRJEB66116) upon manuscript
704 acceptance for publication.

705

706 **Acknowledgements**

707 The authors would like to thank the members of the MPOX Research Consortium UK for the
708 constructive comments and feedback during the preparation of this manuscript. This
709 manuscript is dedicated in memory of Kyriaki Nomikou, an exceptional scientist who sadly
710 passed away during the preparation of this manuscript. Kiki was greatly loved and will be
711 sadly missed by everyone who was blessed to meet her.

712

713 **Funding:**

714 This work was supported by the Biotechnology and Biological Sciences Research Council
715 (BBSRC) Monkeypox rapid response grant (BB/X011607/1) awarded to ADSF, ET, and CB.
716 CD, AH, and ET were funded by the Medical Research Council (MRC; MC_UU_00034/6
717 awarded to ET). KD was funded by the MRC (MC_UU_00034/2 awarded to Pablo Murcia,
718 University of Glasgow). IE, SMF, and CB were funded by the MRC (MC_UU_12014/5 and
719 MC_UU_00034/2 awarded to CB). JKW was funded by an MRC CVR DTA award
720 (MC_ST_U18018). BB was funded by a Wellcome Trust/Royal Society Sir Henry Dale
721 Fellowship (210462/Z/18/Z). QG, VBS, KN, LT, and ADSF were funded by the MRC
722 (MC_UU_00034/6 awarded to ADSF). LO was funded by an MRC precision medicine award
723 (MR/R01566X/1). Patient data and material was collected by the NHS as part of their
724 care and support #DataSavesLives. The data/material used for this study were obtained
725 from ISARIC4C and supported by grants from the the National Institute
726 for Health Research (NIHR; CO-CIN-01), the MRC (MC_PC_19059, MR/X010252/1) and
727 NIHR Clinical Research Network that provided infrastructure support. The funders had no

role in study design, data collection and analysis, decision to publish, or preparation of the manuscript.

Competing interests: The authors declare no competing interests exist.

Author Contributions

Data curation: Chris Davis, Ilaria Epifano, Kieran Dee, Steven McFarlane, Quan Gu, Vattipally B. Sreenu, Lily Tong, Kyriaki Nomikou, Lauren Orr, Chris Boutell.

Formal analysis: Chris Davis, Ilaria Epifano, Kieran Dee, Joanna K. Wojtus, Quan Gu, Vattipally B. Sreenu, Chris Boutell.

Funding acquisition: Benjamin Brennan, Ana Da Silva Filipe, Emma Thomson, Chris Boutell.

Investigation: Chris Davis, Ilaria Epifano, Kieran Dee, Lauren Orr, Antonia Ho, Chris Boutell.

Methodology: Chris Davis, Ilaria Epifano, Steven McFarlane, Benjamin Brennan, Lauren Orr, Chris Boutell.

Project administration: Ana Da Silva Filipe, Antonia Ho, David. A. Barr, Emma Thomson, Chris Boutell.

Resources: Steven McFarlane, Benjamin Brennan, Ana Da Silva Filipe, Antonia Ho, David. A. Barr, Emma Thomson, Chris Boutell.

Supervision: Ana Da Silva Filipe, Emma Thomson, Chris Boutell.

Validation: Chris Davis, Ilaria Epifano, Kieran Dee, Chris Boutell.

Visualization: Chris Davis, Ilaria Epifano, Chris Boutell.

Writing – original draft: Chris Davis, Chris Boutell.

Writing – review & editing: Chris Davis, Ilaria Epifano, Chris Boutell.

References

1 Ulaeto, D. *et al.* New nomenclature for mpox (monkeypox) and monkeypox virus clades. *Lancet Infect Dis* **23**, 273-275, doi:10.1016/S1473-3099(23)00055-5 (2023).

2 Nolen, L. D. *et al.* Introduction of Monkeypox into a Community and Household: Risk Factors and Zoonotic Reservoirs in the Democratic Republic of the Congo. *Am J Trop Med Hyg* **93**, 410-415, doi:10.4269/ajtmh.15-0168 (2015).

3 Huang, Y., Mu, L. & Wang, W. Monkeypox: epidemiology, pathogenesis, treatment and prevention. *Signal Transduct Target Ther* **7**, 373, doi:10.1038/s41392-022-01215-4 (2022).

763 4 El Eid, R., Allaw, F., Haddad, S. F. & Kanj, S. S. Correction: Human monkeypox: A
764 review of the literature. *PLoS Pathog* **18**, e1011008,
765 doi:10.1371/journal.ppat.1011008 (2022).
766 5 Isidro, J. *et al.* Phylogenomic characterization and signs of microevolution in the 2022
767 multi-country outbreak of monkeypox virus. *Nat Med* **28**, 1569-1572,
768 doi:10.1038/s41591-022-01907-y (2022).
769 6 Gigante, C. M. *et al.* Multiple lineages of monkeypox virus detected in the United
770 States, 2021-2022. *Science* **378**, 560-565, doi:10.1126/science.add4153 (2022).
771 7 O'Toole, Á. *et al.* Putative APOBEC3 deaminase editing in MPXV as evidence for
772 sustained human transmission since at least 2016. *bioRxiv*, 2023.2001.2023.525187,
773 doi:10.1101/2023.01.23.525187 (2023).
774 8 Thornhill, J. P. *et al.* Monkeypox Virus Infection in Humans across 16 Countries -
775 April-June 2022. *N Engl J Med* **387**, 679-691, doi:10.1056/NEJMoa2207323 (2022).
776 9 Reynolds, M. G. & Damon, I. K. Outbreaks of human monkeypox after cessation of
777 smallpox vaccination. *Trends Microbiol* **20**, 80-87, doi:10.1016/j.tim.2011.12.001
778 (2012).
779 10 Tarin-Vicente, E. J. *et al.* Clinical presentation and virological assessment of
780 confirmed human monkeypox virus cases in Spain: a prospective observational cohort
781 study. *Lancet* **400**, 661-669, doi:10.1016/S0140-6736(22)01436-2 (2022).
782 11 Fink, D. L. *et al.* Clinical features and management of individuals admitted to hospital
783 with monkeypox and associated complications across the UK: a retrospective cohort
784 study. *Lancet Infect Dis*, doi:10.1016/S1473-3099(22)00806-4 (2022).
785 12 Palich, R. *et al.* Viral loads in clinical samples of men with monkeypox virus
786 infection: a French case series. *Lancet Infect Dis* **23**, 74-80, doi:10.1016/S1473-
787 3099(22)00586-2 (2023).
788 13 Mailhe, M. *et al.* Clinical characteristics of ambulatory and hospitalized patients with
789 monkeypox virus infection: an observational cohort study. *Clin Microbiol Infect*,
790 doi:10.1016/j.cmi.2022.08.012 (2022).
791 14 Jezek, Z., Szczeniowski, M., Paluku, K. M. & Mutombo, M. Human monkeypox:
792 clinical features of 282 patients. *J Infect Dis* **156**, 293-298,
793 doi:10.1093/infdis/156.2.293 (1987).
794 15 McCollum, A. M. & Damon, I. K. Human monkeypox. *Clin Infect Dis* **58**, 260-267,
795 doi:10.1093/cid/cit703 (2014).
796 16 Huhn, G. D. *et al.* Clinical characteristics of human monkeypox, and risk factors for
797 severe disease. *Clin Infect Dis* **41**, 1742-1751, doi:10.1086/498115 (2005).
798 17 Yinka-Ogunleye, A. *et al.* Outbreak of human monkeypox in Nigeria in 2017-18: a
799 clinical and epidemiological report. *Lancet Infect Dis* **19**, 872-879,
800 doi:10.1016/S1473-3099(19)30294-4 (2019).
801 18 Tofan, V., Lenghel, A., de Camargo, M. M. & Stan, R. C. Fever as an evolutionary
802 agent to select immune complexes interfaces. *Immunogenetics* **74**, 465-474,
803 doi:10.1007/s00251-022-01263-8 (2022).
804 19 Becskei, A. & Rahaman, S. The life and death of RNA across temperatures. *Comput*
805 *Struct Biotechnol J* **20**, 4325-4336, doi:10.1016/j.csbj.2022.08.008 (2022).
806 20 Evans, S. S., Repasky, E. A. & Fisher, D. T. Fever and the thermal regulation of
807 immunity: the immune system feels the heat. *Nat Rev Immunol* **15**, 335-349,
808 doi:10.1038/nri3843 (2015).
809 21 Ogoina, D. Fever, fever patterns and diseases called 'fever'--a review. *J Infect Public*
810 *Health* **4**, 108-124, doi:10.1016/j.jiph.2011.05.002 (2011).
811 22 Alcami, A. & Smith, G. L. A mechanism for the inhibition of fever by a virus. *Proc*
812 *Natl Acad Sci U S A* **93**, 11029-11034, doi:10.1073/pnas.93.20.11029 (1996).

23 Laloli, L. *et al.* Time-resolved characterization of the innate immune response in the respiratory epithelium of human, porcine, and bovine during influenza virus infection. *Front Immunol* **13**, 970325, doi:10.3389/fimmu.2022.970325 (2022).
24 V'Kovski, P. *et al.* Disparate temperature-dependent virus-host dynamics for SARS-CoV-2 and SARS-CoV in the human respiratory epithelium. *PLoS Biol* **19**, e3001158, doi:10.1371/journal.pbio.3001158 (2021).
25 Dalton, R. M. *et al.* Temperature sensitive influenza A virus genome replication results from low thermal stability of polymerase-cRNA complexes. *Virol J* **3**, 58, doi:10.1186/1743-422X-3-58 (2006).
26 Herder, V. *et al.* Elevated temperature inhibits SARS-CoV-2 replication in respiratory epithelium independently of IFN-mediated innate immune defenses. *PLoS Biol* **19**, e3001065, doi:10.1371/journal.pbio.3001065 (2021).
27 Earn, D. J., Andrews, P. W. & Bolker, B. M. Population-level effects of suppressing fever. *Proc Biol Sci* **281**, 20132570, doi:10.1098/rspb.2013.2570 (2014).
28 Ryan, M. & Levy, M. M. Clinical review: fever in intensive care unit patients. *Crit Care* **7**, 221-225, doi:10.1186/cc1879 (2003).
29 Schulman, C. I. *et al.* The effect of antipyretic therapy upon outcomes in critically ill patients: a randomized, prospective study. *Surg Infect (Larchmt)* **6**, 369-375, doi:10.1089/sur.2005.6.369 (2005).
30 Hutson, C. L. *et al.* A prairie dog animal model of systemic orthopoxvirus disease using West African and Congo Basin strains of monkeypox virus. *J Gen Virol* **90**, 323-333, doi:10.1099/vir.0.005108-0 (2009).
31 Hutson, C. L. *et al.* Laboratory Investigations of African Pouched Rats (Cricetomys gambianus) as a Potential Reservoir Host Species for Monkeypox Virus. *PLoS Negl Trop Dis* **9**, e0004013, doi:10.1371/journal.pntd.0004013 (2015).
32 Tree, J. A. *et al.* Sequence of pathogenic events in cynomolgus macaques infected with aerosolized monkeypox virus. *J Virol* **89**, 4335-4344, doi:10.1128/JVI.03029-14 (2015).
33 Bedson, H. S. & Dumbell, K. R. The effect of temperature on the growth of pox viruses in the chick embryo. *J Hyg (Lond)* **59**, 457-469, doi:10.1017/s0022172400039152 (1961).
34 Dumbell, K. R. & Bedson, H. S. The Use of Ceiling Temperature and Reactivation in the Isolation of Pox Virus Hybrids. *J Hyg (Lond)* **62**, 133-140, doi:10.1017/s0022172400039863 (1964).
35 Molteni, C., Forni, D., Cagliani, R., Clerici, M. & Sironi, M. Genetic ancestry and population structure of vaccinia virus. *NPJ Vaccines* **7**, 92, doi:10.1038/s41541-022-00519-4 (2022).
36 Senkevich, T. G., Yutin, N., Wolf, Y. I., Koonin, E. V. & Moss, B. Ancient Gene Capture and Recent Gene Loss Shape the Evolution of Orthopoxvirus-Host Interaction Genes. *mBio* **12**, e0149521, doi:10.1128/mBio.01495-21 (2021).
37 Qin, L., Liang, M. & Evans, D. H. Genomic analysis of vaccinia virus strain TianTan provides new insights into the evolution and evolutionary relationships between Orthopoxviruses. *Virology* **442**, 59-66, doi:10.1016/j.virol.2013.03.025 (2013).
38 Thompson, R. L. & Coates, M. S. The Effect of Temperature upon the Growth and Survival of Myxoma, Herpes, and Vaccinia Viruses in Tissue Culture. *The Journal of Infectious Diseases* **71**, 83-85, doi:10.1093/infdis/71.1.83 (1942).
39 Forni, D., Cagliani, R., Pozzoli, U. & Sironi, M. An APOBEC3 Mutational Signature in the Genomes of Human-Infecting Orthopoxviruses. *mSphere* **8**, e0006223, doi:10.1128/msphere.00062-23 (2023).

862 40 Suspene, R. *et al.* APOBEC3F is a mutational driver of the human Monkeypox virus
863 identified in the 2022 outbreak. *J Infect Dis*, doi:10.1093/infdis/jiad165 (2023).
864 41 Moein, S., Javanmard, S. H., Abedi, M., Izadpanahi, M. H. & Gheisari, Y.
865 Identification of Appropriate Housekeeping Genes for Gene Expression Analysis in
866 Long-term Hypoxia-treated Kidney Cells. *Adv Biomed Res* **6**, 15, doi:10.4103/2277-
867 9175.200790 (2017).
868 42 Curina, A. *et al.* High constitutive activity of a broad panel of housekeeping and
869 tissue-specific cis-regulatory elements depends on a subset of ETS proteins. *Genes*
870 *Dev* **31**, 399-412, doi:10.1101/gad.293134.116 (2017).
871 43 Eisenberg, E. & Levanon, E. Y. Human housekeeping genes, revisited. *Trends Genet*
872 **29**, 569-574, doi:10.1016/j.tig.2013.05.010 (2013).
873 44 Lum, F. M. *et al.* Monkeypox: disease epidemiology, host immunity and clinical
874 interventions. *Nat Rev Immunol* **22**, 597-613, doi:10.1038/s41577-022-00775-4
875 (2022).
876 45 Li, H. *et al.* The land-scape of immune response to monkeypox virus. *EBioMedicine*
877 **87**, 104424, doi:10.1016/j.ebiom.2022.104424 (2023).
878 46 Johnston, S. C. *et al.* Cytokine modulation correlates with severity of monkeypox
879 disease in humans. *J Clin Virol* **63**, 42-45, doi:10.1016/j.jcv.2014.12.001 (2015).
880 47 Joklik, W. K., Abel, P. & Holmes, I. H. Reactivation of poxviruses by a non-genetic
881 mechanism. *Nature* **186**, 992-993, doi:10.1038/186992b0 (1960).
882 48 Sood, C. L. & Moss, B. Vaccinia virus A43R gene encodes an orthopoxvirus-specific
883 late non-virion type-1 membrane protein that is dispensable for replication but
884 enhances intradermal lesion formation. *Virology* **396**, 160-168,
885 doi:10.1016/j.virol.2009.10.025 (2010).
886 49 Tanaka-Kataoka, M. *et al.* In vivo antiviral effect of interleukin 18 in a mouse model
887 of vaccinia virus infection. *Cytokine* **11**, 593-599, doi:10.1006/cyto.1998.0453 (1999).
888 50 Symons, J. A. *et al.* The vaccinia virus C12L protein inhibits mouse IL-18 and
889 promotes virus virulence in the murine intranasal model. *J Gen Virol* **83**, 2833-2844,
890 doi:10.1099/0022-1317-83-11-2833 (2002).
891 51 Clark, R. H., Kenyon, J. C., Bartlett, N. W., Tscharke, D. C. & Smith, G. L. Deletion
892 of gene A41L enhances vaccinia virus immunogenicity and vaccine efficacy. *J Gen*
893 *Virol* **87**, 29-38, doi:10.1099/vir.0.81417-0 (2006).
894 52 El-Radhi, A. S. in *Clinical Manual of Fever in Children* (ed A. Sahib El-Radhi) 53-
895 68 (Springer International Publishing, 2018).
896 53 Johnston, S. C. *et al.* In vitro inhibition of monkeypox virus production and spread by
897 Interferon-beta. *Virol J* **9**, 5, doi:10.1186/1743-422X-9-5 (2012).
898 54 Stabenow, J. *et al.* A mouse model of lethal infection for evaluating prophylactics and
899 therapeutics against Monkeypox virus. *J Virol* **84**, 3909-3920,
900 doi:10.1128/JVI.02012-09 (2010).
901 55 Arndt, W. D. *et al.* Evasion of the Innate Immune Type I Interferon System by
902 Monkeypox Virus. *J Virol* **89**, 10489-10499, doi:10.1128/JVI.00304-15 (2015).
903 56 Hernaez, B. *et al.* A virus-encoded type I interferon decoy receptor enables evasion of
904 host immunity through cell-surface binding. *Nat Commun* **9**, 5440,
905 doi:10.1038/s41467-018-07772-z (2018).
906 57 Arndt, W. D. *et al.* Monkeypox virus induces the synthesis of less dsRNA than
907 vaccinia virus, and is more resistant to the anti-poxvirus drug, IBT, than vaccinia
908 virus. *Virology* **497**, 125-135, doi:10.1016/j.virol.2016.07.016 (2016).
909 58 Conn, K. L. *et al.* Novel Role for Protein Inhibitor of Activated STAT 4 (PIAS4) in
910 the Restriction of Herpes Simplex Virus 1 by the Cellular Intrinsic Antiviral Immune
911 Response. *J Virol* **90**, 4807-4826, doi:10.1128/JVI.03055-15 (2016).

59 Piboonniyom, S. O. *et al.* Abrogation of the retinoblastoma tumor suppressor checkpoint during keratinocyte immortalization is not sufficient for induction of centrosome-mediated genomic instability. *Cancer Res* **63**, 476-483 (2003).
60 Meyers, C. Organotypic (raft) epithelial tissue culture system for the differentiation-dependent replication of papillomavirus. *Methods in Cell Science* **18**, 201-210, doi:10.1007/BF00132885 (1996).
61 Carter, G. C. *et al.* Vaccinia virus cores are transported on microtubules. *J Gen Virol* **84**, 2443-2458, doi:10.1099/vir.0.19271-0 (2003).
62 Kotwal, G. J. & Abrahams, M.-R. in *Vaccinia Virus and Poxvirology: Methods and Protocols* (ed Stuart N. Isaacs) 101-112 (Humana Press, 2004).
63 Everett, R. D., Boutell, C. & Orr, A. Phenotype of a herpes simplex virus type 1 mutant that fails to express immediate-early regulatory protein ICP0. *J Virol* **78**, 1763-1774, doi:10.1128/jvi.78.4.1763-1774.2004 (2004).
64 Katoh, K., Misawa, K., Kuma, K. & Miyata, T. MAFFT: a novel method for rapid multiple sequence alignment based on fast Fourier transform. *Nucleic Acids Res* **30**, 3059-3066, doi:10.1093/nar/gkf436 (2002).
65 Baker, J. L. & Ward, B. M. Development and comparison of a quantitative TaqMan-MGB real-time PCR assay to three other methods of quantifying vaccinia virions. *J Virol Methods* **196**, 126-132, doi:10.1016/j.jviromet.2013.10.026 (2014).
66 Davi, S. D. *et al.* Recombinase polymerase amplification assay for rapid detection of Monkeypox virus. *Diagn Microbiol Infect Dis* **95**, 41-45, doi:10.1016/j.diagmicrobio.2019.03.015 (2019).
67 Kim, D., Langmead, B. & Salzberg, S. L. HISAT: a fast spliced aligner with low memory requirements. *Nat Methods* **12**, 357-360, doi:10.1038/nmeth.3317 (2015).
68 Liao, Y., Smyth, G. K. & Shi, W. featureCounts: an efficient general purpose program for assigning sequence reads to genomic features. *Bioinformatics* **30**, 923-930, doi:10.1093/bioinformatics/btt656 (2014).
69 Robinson, M. D., McCarthy, D. J. & Smyth, G. K. edgeR: a Bioconductor package for differential expression analysis of digital gene expression data. *Bioinformatics* **26**, 139-140, doi:10.1093/bioinformatics/btp616 (2010).
70 Fabregat, A. *et al.* The Reactome Pathway Knowledgebase. *Nucleic Acids Res* **46**, D649-D655, doi:10.1093/nar/gkx1132 (2018).
71 Jassal, B. *et al.* The reactome pathway knowledgebase. *Nucleic Acids Res* **48**, D498-D503, doi:10.1093/nar/gkz1031 (2020).
72 Zhou, Y. *et al.* Metascape provides a biologist-oriented resource for the analysis of systems-level datasets. *Nat Commun* **10**, 1523, doi:10.1038/s41467-019-09234-6 (2019).
73 Shaw, A. E. *et al.* Fundamental properties of the mammalian innate immune system revealed by multispecies comparison of type I interferon responses. *PLoS Biol* **15**, e2004086, doi:10.1371/journal.pbio.2004086 (2017).

Figure Legends

Fig 1. Clinical MPXV isolation and genotyping. Skin swabs obtained from a hospitalised MPXV PCR-positive patient presenting with fever and rash during the 2022 mpox outbreak

959 were used to isolate and amplify infectious virus. Clinical swabs (CVR_MPXV1a) and
960 supernatant derived from primary amplification (MPXV CVR_S1) were subjected to
961 Illumina sequencing and confirmed to be identical (accession number ON808413). (A)
962 Phylogenetic tree highlighting the evolutionary and taxonomic relationship of MPXV
963 CVR_S1 (red text) to other sequenced MPXV Clade IIa and IIb strains (as indicated). (B)
964 Schematic diagram highlighting the position and distribution of the 67 single nucleotide
965 polymorphisms (SNPs; supplemental S1 data) identified within the MPXV CVR_S1 genome
966 relative to the MPXV Clade IIa reference strain (NC_063383-A; blue text) used for genome
967 annotation throughout the study. Blue lines (guanine to adenine, G to A), red lines (cytosine
968 to thymine, C to T), yellow lines (adenine to guanine, A to G), green lines (thymine to
969 cytosine, T to C).
970
971 **Fig 2. Tissue temperature influences the outcome of MPXV replication in skin**
972 **epithelium.** Human keratinocytes were differentiated into pseudostratified skin epithelium
973 under air liquid interface (ALI) for 12 to 14 days. Tissues were mock treated or MPXV
974 infected (MOI 10^2 or 10^3 PFU/tissue) for 1 h at 37 °C prior to incubation at 33, 37, or 40 °C
975 for 72 h (as indicated). (A) Representative immunohistochemistry (IHC) stained tissue
976 sections counter-stained with haematoxylin. Brown highlights epithelial regions positive for
977 MPXV virion antigen expression. Scale bar 0.25 mm. (B) Quantitation of epithelial thickness
978 of mock treated or MPXV infected tissues (as in A). Mean and 95% CI shown. Values
979 derived from a minimum of 40 measurements per tissue; *p*-values shown, Kruskal-Wallis
980 one-way ANOVA. (C) Quantitation of MPXV infected tissue area. Values normalised to
981 infected tissues incubated at 37 °C. Mean and SD shown. (D) Proportion of weak, moderate,
982 and strong MPXV virion antigen positive cells. Values normalised to the proportion of strong
983 MPXV antigen-stained cells from infected tissues incubated at 37 °C per biological
984 experiment. (C/D) *P*-values shown, one sample two-tailed t test against a theoretical mean of
985 1. (A to D) *N*=3 independent biological experiments. Raw values presented in supplemental
986 S2 data. Original tissue section scans shown in Fig S1.
987
988 **Fig 3. Temperature elevation inhibits MPXV replication.** Human foreskin fibroblast (HFt)
989 cells were infected with VACV (MOI 0.0005 or 0.1 PFU/cell, A to D or E, respectively; top
990 panels) or MPXV (MOI 0.001 or 0.1 PFU/cell, F to I or J, respectively; bottom panels) for 1
991 h at 37 °C prior to incubation at 33, 37, 38.5 or 40 °C. (A/F) Representative images of VACV
992 or MPXV infected cell monolayers stained with Coomassie Brilliant blue at 48 h post-

993 infection (hpi). (B/G) Quantitation of VACV or MPXV plaque counts at 48 hpi. Means and
994 SD shown; *p*-values shown, Dunnett's unpaired one-way ANOVA. (C/H) Quantitation of
995 plaque diameters at 48 hpi. Values normalised to the geometric mean at 33 °C per biological
996 experiment. Means and 95% CI shown; *p*-values shown, Kruskai-Wallis one-way ANOVA.
997 (D/I) Quantitation (log10 PFU/ml) of cell-released virus from infected HFt cells quantified
998 by plaque assay in Vero E6 cells. Mean and SD shown; *p*-values shown, Dunnett's unpaired
999 one-way ANOVA. Limit of detection (LOD) shown (dotted grey line). (E/F) qPCR
1000 quantitation of virus host-cell entry at 1 hpi. Values normalised to 37 °C per biological
1001 experiment. All data points shown; line, mean; whisker, SD; *p*-values shown, one sample
1002 two-tailed t test against a theoretical mean of 1. (A to J) $N \geq 3$ independent biological
1003 experiments. Raw values presented in supplemental S3 data.
1004
1005 **Fig 4. Basal host-cell temperature influences MPXV replication in a cell-type dependent**
1006 **manner.** Confluent HFt, NOK (human normal oral keratinocyte), RPE (human retinal
1007 pigmented epithelial), Vero E6 (green monkey kidney epithelial), or CV-1 (green monkey
1008 kidney fibroblast) cell monolayers were infected with VACV (MOI 0.0005 PFU/cell; top
1009 panels) or MPXV (MOI 0.001 PFU/cell; bottom panels) for 1 h at 37 °C prior to incubation at
1010 33, 37, 38.5 or 40 °C. Infected cell monolayers were stained with Coomassie Brilliant blue at
1011 48 h post-infection and plaque counts quantified. Values were normalised to 37 °C per cell
1012 line per biological experiment (grey dotted line). (A/C) Normalised plaque counts per cell
1013 line over the temperature range of analysis. Means and SD shown; *p*-values shown, one
1014 sample two-tailed t test against a theoretical mean of 1. (B/D) Normalised plaque counts per
1015 temperature condition. Means and SD shown; *p*-values shown, Dunnett's unpaired one-way
1016 ANOVA. (A to D) $N=3$ independent biological experiments. Raw values presented in
1017 supplemental S4 data.
1018
1019 **Fig 5. Basal host-cell temperature differentially influences the regulation of MPXV**
1020 **transcription.** HFt cells were infected with MPXV (MOI 0.01 PFU/cell) for 1 h at 37 °C
1021 prior to incubation at 33, 37, 38.5 or 40 °C. RNA was extracted at 48 h post-infection (hpi)
1022 for RNA-Seq. Viral reads were aligned to the MPXV reference sequence (NC_063383.1) and
1023 normalised to counts per million (CPM) and used to quantify MPXV transcript expression
1024 levels per ORF. (A) Principal Component (PC) analysis of MPXV ORF transcript expression
1025 levels per incubation temperature. (B) Line graph showing CPM per ORF (log10). Purple
1026 circles and text highlight viral ORFs < 1 CPM (dotted line). (C) Expression level of MPXV

1027 ORFs (log2 CPM); every third ORF labelled. (D) Expression level of MPXV ORFs relating
1028 to the viral RNA (vRNA) polymerase complex, viral toll like receptor (vTLR) antagonists,
1029 and intracellular mature virus (IMV) assembly (as indicated). Purple text highlights viral
1030 ORFs < 1 CPM per ORF (as in B). (E) Line graph showing normalised CPM count per ORF
1031 (log2 CPM) at 33 and 38.5 °C. Values were normalised to CPM counts at 37 °C (solid grey
1032 line). Orange circles and text highlight viral ORFs ≥ 1.5 log2 FC (fold change) relative to 37
1033 °C (dotted grey line). (A to E) *N*=3 independent biological experiments; *p*-values shown,
1034 Dunnett's paired one-way ANOVA (bottom), paired two-tailed *t* test (top). Raw values
1035 presented in supplemental S5 data.
1036
1037 **Fig 6. Basal temperature influences the host-cell response to MPXV infection.** HFt cells
1038 were mock treated or infected with MPXV (MOI 0.01 PFU/cell) for 1 h at 37 °C prior to
1039 incubation at 33, 37, 38.5 or 40 °C. RNA was extracted at 48 h post-infection (hpi) for RNA-
1040 Seq. Host mapped reads were aligned to the human genome, normalised to counts per million
1041 (CPM), and DEGs (FDR < 0.05, ≥ 1.5 log2 FC) identified for each paired condition analysed
1042 (as indicated). (A) Venn diagram showing the number of unique or shared DEGs between
1043 each paired condition. (B) Circos plots showing the proportion of unique (light orange inner
1044 circle) or shared (dark orange inner circle + purple lines) DEGs between each paired
1045 condition. (C) Metascape pathway analysis showing significant up-regulated DEG
1046 enrichment (*p*-value < 0.05; log10 *p*-values shown) for each paired condition (as in A/B).
1047 Black arrows highlight enriched for cytokine related pathways; grey boxes, *p*-value > 0.05.
1048 (D) Expression level (log2 CPM) of cytokine related DEGs identified to be upregulated in
1049 response to MPXV infection (black arrows in C, 71 genes in total; log2 CPM). (E) Principal
1050 Component (PC) analysis of cytokine related DEGs (as in D) in mock treated and MPXV
1051 infected cells (as indicated). Purple arrow highlights MPXV 40 °C expression levels
1052 clustering with mock treated samples. (F) Expression profile of cytokine related DEGs (as in
1053 D). Black line, median; whisker, 95% CI; all data points shown. (G) Expression level (log2
1054 CPM) of host interferon (IFN)-related receptors and cytokines in mock treated or MPXV
1055 infected cells. Black arrow highlights expression level of *IFNB1* in mock treated or MPXV
1056 infected cells. (D, F, G) *P*-values shown, Dunnett's paired one-way ANOVA. (A to G) *N*=3
1057 independent biological experiments. Raw values presented in supplemental S6 data.
1058
1059 **Fig 7. Basal host-cell temperature influences the interleukin response to MPXV**
1060 **infection.** HFt cells were mock treated or infected with MPXV (MOI 0.01 PFU/cell) for 1 h

1061 at 37 °C prior to incubation at 33, 37, 38.5 or 40 °C. RNA was extracted at 48 h post-
1062 infection (hpi) for RNA-Seq. Host mapped reads were aligned to the human genome,
1063 normalised to counts per million (CPM), and DEGs (FDR < 0.05, ≥ 1.5 log2 FC) identified.
1064 (A) Scatter plot showing DEGs identified between MPXV infected cells incubated at 37 and
1065 40 °C; up-regulated, red circles; down-regulated, blue circles. (B) Reactome pathway
1066 analysis of down-regulated mapped DEGs (blue circles in A). Top 25 down-regulated
1067 pathways (FDR < 0.05) shown (blue bars; plotted as -log10 FDR). Dotted line, threshold of
1068 significance (-log10 FDR of 0.05). Pathways relating to cell cycle (grey arrow and circle) and
1069 immune system regulation (coloured arrows and circles) are highlighted. (C) Venn diagram
1070 showing the number of unique or shared DEGs identified in immune system pathways
1071 (coloured arrows and circles identified in B). (D) Expression level (log2 CPM) of immune
1072 system DEGs (identified in B; 61 genes in total); *p*-values shown, Dunnett's unpaired one-
1073 way ANOVA (top), unpaired two-tailed *t* test (bottom). DEGs associated with Signalling by
1074 Interleukins (ILs) highlighted (green circles). (E) Expression profile (CPM) of selected
1075 interleukins (IL6, IL11, and IL12A) and chemokines (CXCL1, CXCL6, CXCL2, CXCL3) in
1076 mock treated (grey lines) and MPXV infected (green lines) cells across the temperature range
1077 of analysis; *p*-values shown, unpaired two-tailed *t* test. Raw values presented in supplemental
1078 S7 Data.
1079
1080 **Fig 8. Temperature elevation enhances the type-I IFN-mediated host-cell restriction of**
1081 **MPXV.** (A to D) HFt cells were pre-treated with IFN-β (0 to 100 IU/ml, as indicated) for 16
1082 h at 33, 37, 38.5 or 40 °C prior to MPXV (MOI 0.001 PFU/cell) infection (1 h at 37 °C) and
1083 continued incubation at their respective incubation temperatures in the presence of IFN. (A)
1084 Representative images of MPXV infected cell monolayers pre-treated with IFN and stained
1085 with Coomassie Brilliant blue at 48 h post-infection (hpi). (B) Quantitation of MPXV plaque
1086 counts at 48 hpi (as shown in A). Means and SD shown. Grey dotted lines and circles
1087 highlight absence of plaque formation at 40 °C. (C/D) Relative MPXV plaque counts. Values
1088 were normalised to no IFN treatment (dotted grey line) per incubation temperature. (C)
1089 Means and SD shown; coloured lines and text, linear regression and corresponding R^2 values.
1090 (D) As in C, all data points shown; black line, mean; whisker, SD; *p*-values shown, Dunnett's
1091 unpaired one-way ANOVA. (E to J) Naïve HFt cells were infected with MPXV (MOI 0.01
1092 PFU/cell) for 1 h at 37 °C prior to overlay with media containing IFN-β (0 to 200 IU/ml, as
1093 indicated) and incubation at 33, 37, 38.5 or 40 °C. (E/F) Cells were fixed at 24 h and stained

1094 for MPXV virion protein expression and the number of antigen positive cells quantified by
1095 indirect immunofluorescence. (E) Mean MPXV positive cell counts (x100) per infected cell
1096 monolayer. (F) As in E, mean and SD shown. (G to J) Infected or infected and IFN treated
1097 monolayers incubated at 37 or 40 °C were either fixed at 48 h or washed twice and overlayed
1098 with fresh media (IFN washout) and incubation at 37 °C for an additional 48 h prior to
1099 fixation at Coomassie Brilliant blue staining. (G) Quantitation of MPXV plaque counts in cell
1100 monolayers incubated at 40 °C or temperature downshifted from 40 to 37 °C (40>37) with
1101 continued incubation. (H) Quantitation of MPXV plaque counts in cell monolayers incubated
1102 at 37 °C in the presence of IFN or following IFN washout and continued incubation. All data
1103 points shown. (J) Quantitation of MPXV plaque counts in cell monolayers incubated at 37 or
1104 40 °C in the presence of IFN (1 to 200 IU/ml, as indicated) with IFN washout at 48 h and
1105 continued incubation at 37 °C (no IFN). All data points shown. (G to J) Values were
1106 normalised to plaque counts determined at 37 °C (no IFN treatment at 48 h). Mean and SD
1107 shown; *p*-values shown, unpaired two-tailed *t* test. Raw values presented in supplemental S8
1108 Data.
1109
1110 **Fig S1. Tissue temperature influences the outcome of MPXV replication in skin**
1111 **epithelium.** Human keratinocytes were seed onto fibroblast-containing collagen coated 6.5
1112 mm transwells and differentiated under ALI for 14 days. Pseudostratified skin epithelium
1113 cultures were mock treated (media only) or MPXV infected (MOI 10^2 or 10^3 PFU/tissue) for
1114 1 h at 37 °C prior to incubation at 33, 37, or 40 °C (as indicated) for 72 h. Whole tissue
1115 sections were stained for MPXV virion antigen expression by immunohistochemistry and
1116 counter stained with eosin. Scale bar = 0.5 mm.
1117
1118 **Fig S2. Temperature elevation inhibits OPXV replication.** (A) Quantitation of DAPI
1119 stained nuclei in mock treated HFt cells incubated at 33, 37, 38.5 or 40 °C for 48 h. (B) MTS
1120 cell viability assay of mock treated or puromycin (Puro, 1 □g/ml; positive death control)
1121 treated HFt cells incubated at 37 or 40 °C for 24 h (as indicated). (C to E) Confluent HFt
1122 (human foreskin fibroblast), NOK (human normal oral keratinocyte), RPE (human retinal
1123 pigmented epithelial), Vero E6 (green monkey kidney epithelial), or CV-1 (green monkey
1124 kidney fibroblast) cell monolayers were infected with (C) HSV-1 (MOI 0.002 PFU/cell), (D)
1125 VACV (MOI 0.0005 PFU/cell), or (E) MPXV (MOI 0.001 PFU/cell) for 1 h at 37 °C prior to
1126 overlay and incubation at 33, 37, 38.5 or 40 °C. Infected cell monolayers were fixed at 48 h

1127 and stained with Coomassie Brilliant blue. (C) Quantitation of HSV-1 plaque counts in HFt
1128 cells over the temperature incubation range of analysis. Values were normalised to plaque
1129 counts at 37 °C. Means and SD shown; *p*-values shown, one sample two-tailed t test against a
1130 theoretical mean of 1. (D/E) Representative images of VACV or MPXV infected HFT, RPE,
1131 NOK, Vero E6 (Meso), and CV-1 cell monolayers stained with Coomassie Brilliant blue at
1132 48 h post-infection (hpi). (A to E) $N \geq 3$ independent biological experiments. Raw values
1133 presented in supplemental S9 data.
1134
1135 **Fig S3. Basal host-cell temperature differentially influences the regulation of MPXV**
1136 **transcription.** HFt cells were infected with MPXV (MOI 0.01 PFU/cell) for 1 h at 37 °C
1137 prior to incubation at 33, 37, 38.5 or 40 °C. RNA was extracted at 48 h post-infection (hpi)
1138 for RNA-Seq. Host sequences were aligned to the human genome and mapped read (MR)
1139 counts normalised to counts per million (CPM). Viral sequences were aligned to the MPXV
1140 reference sequence (NC_063383.1) and viral MR counts used to quantify MPXV transcript
1141 abundance. (A) Expression level (log2 CPM) of 28 host reference genes over the temperature
1142 range of analysis. (B) Host MR counts in mock treated (grey bars) and MPXV infected
1143 (green bars) cells over the temperature range of analysis. (C) Viral MR counts in MPXV
1144 infected cells over the temperature range of analysis. (A to C) $N=3$ independent biological
1145 experiments; *p*-values shown, unpaired Dunnett's one-way ANOVA. Raw values presented
1146 in supplemental S10 data.
1147
1148 **Fig S4. MPXV infection does not stimulate the induction of the type-I IFN response.** HFt
1149 cells were mock treated or infected with MPXV (MOI 0.01 PFU/cell) for 1 h at 37 °C prior to
1150 incubation at 33, 37, 38.5 or 40 °C. RNA was extracted at 48 h post-infection (hpi) for RNA-
1151 Seq. Host sequences were aligned to the human genome and mapped read (MR) counts
1152 normalised to counts per million (CPM). (A) Expression level (log2 CPM) of host interferon
1153 (IFN)-related receptors and cytokines in mock treated or MPXV infected cells over the
1154 temperature range of analysis. (B) Expression profile (CPM) of IFNB1 (circles) and IL-6
1155 (squares) transcript levels in mock treated (grey lines) or MPXV infected (pink lines) cells
1156 over the temperature range of analysis. Means and SD shown. (C/D) Expression profile (log2
1157 CPM) of 489 interferon responsive genes previously identified to be upregulated in response
1158 to universal interferon[73]; every 8th gene labelled. Grey lines in C highlight profile similarity
1159 between experimental conditions. (E) Expression profile (log2 CPM) of host genes associated
1160 with Cytokine Signalling in Immune System (R-HAS-1280215; 715 genes in total) in mock

1161 treated or MPXV infected cells over the temperature range of analysis. (F) Expression profile
1162 (log2 CPM) of host genes associated with Signalling by Interleukins (R-HAS-449147; 459
1163 genes in total) in mock treated or MPXV infected cells over the temperature range of
1164 analysis. (A to G) *N*=3 independent biological experiments. Raw values presented in
1165 supplemental S11 data. (D to F) *P*-values shown, Dunnett's paired one-way ANOVA with
1166 Giesser-Greenhouse correction.
1167
1168 **Fig S5. Temperature elevation enhances the type-I IFN-mediated host-cell restriction of**
1169 **VACV.** (A to D) HFt cells were pre-treated with IFN-β (0 to 100 IU/ml, as indicated) for 16
1170 h at 33, 37, 38.5 or 40 °C prior to VACV (MOI 0.0005 PFU/cell) infection (1 h at 37 °C) and
1171 continued incubation at their respective temperatures in the presence of IFN. (A)
1172 Representative images of VACV infected cell monolayers pre-treated with IFN and stained
1173 with Coomassie Brilliant blue at 48 h post-infection (hpi). (B) Quantitation of VACV plaque
1174 counts at 48 hpi (as shown in A). Means and SD shown. (C/D) Relative VACV plaque
1175 counts). Values were normalised to no IFN treatment (dotted grey line) per incubation
1176 temperature. (C) Means and SD shown; coloured lines and text, linear regression and
1177 corresponding R^2 values. (D) As in C, all data points shown; black line, mean; whisker, SD;
1178 *p*-values shown, Dunnett's unpaired one-way ANOVA. (E to J) Naïve HFt cells were
1179 infected with VACV (MOI 0.01 PFU/cell, E and F; MOI 0.0005 PFU/cell, G to J) for 1 h at
1180 37 °C prior to overlay with media containing IFN-β (0 to 200 IU/ml, as indicated) and
1181 incubation at 33, 37, 38.5 or 40 °C. (E/F) Cells were fixed at 24 h and stained for VACV
1182 virion protein expression and the number of antigen positive cells quantified by indirect
1183 immunofluorescence. (E) Mean VACV positive cell counts (x1000) per infected cell
1184 monolayer. (F) As in E, mean and SD shown. (G to J) Infected or infected and IFN treated
1185 monolayers incubated at 37 or 40 °C were either fixed at 24 h or washed and overlayed with
1186 fresh media (IFN washout) and incubation at 37 °C for an additional 24 h prior to fixation
1187 and staining. (G) Quantitation of VACV plaque counts in cell monolayers incubated at 40 °C
1188 or temperature downshifted from 40 to 37 °C (40>37) with continued incubation for 24 h. (H)
1189 Quantitation of VACV plaque counts in cell monolayers incubated at 37 or 40 °C in the
1190 presence of IFN (red and blues circles plus solid lines, respectively) or following IFN
1191 washout and continued incubation at 37 °C for 24 h (red and blue squares plus dotted lines,
1192 respectively). (J) Values presented for IFN washout and continued incubation at 37 °C for 24
1193 (red and blue squares in H), all data points shown. (G to J) Values were normalised to plaque

1194 counts determined at 37 °C (no IFN treatment at 24 h). Mean and SD shown; *p*-values shown,
1195 unpaired two-tailed *t* test. Raw values presented in supplemental S12 Data.
1196

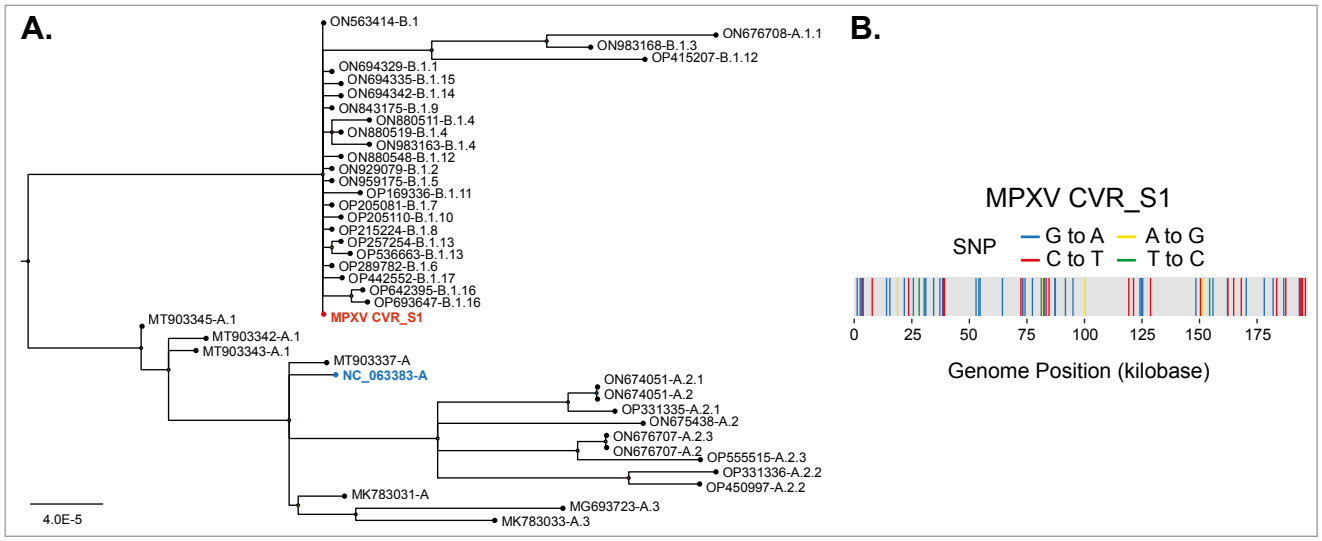

Figure 1. Clinical MPOX virus isolation and genotyping.

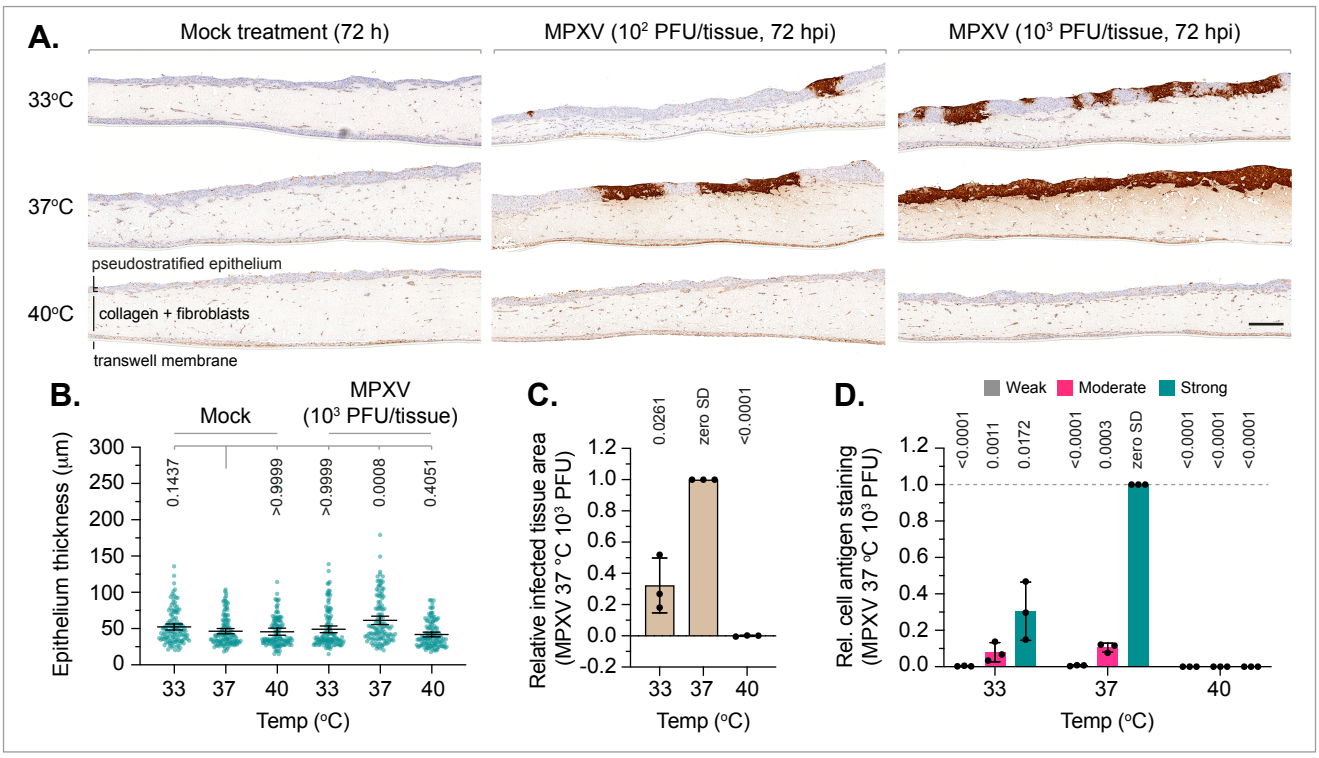

Figure 2. Tissue temperature influences the outcome of MPXV infection in skin epithelium

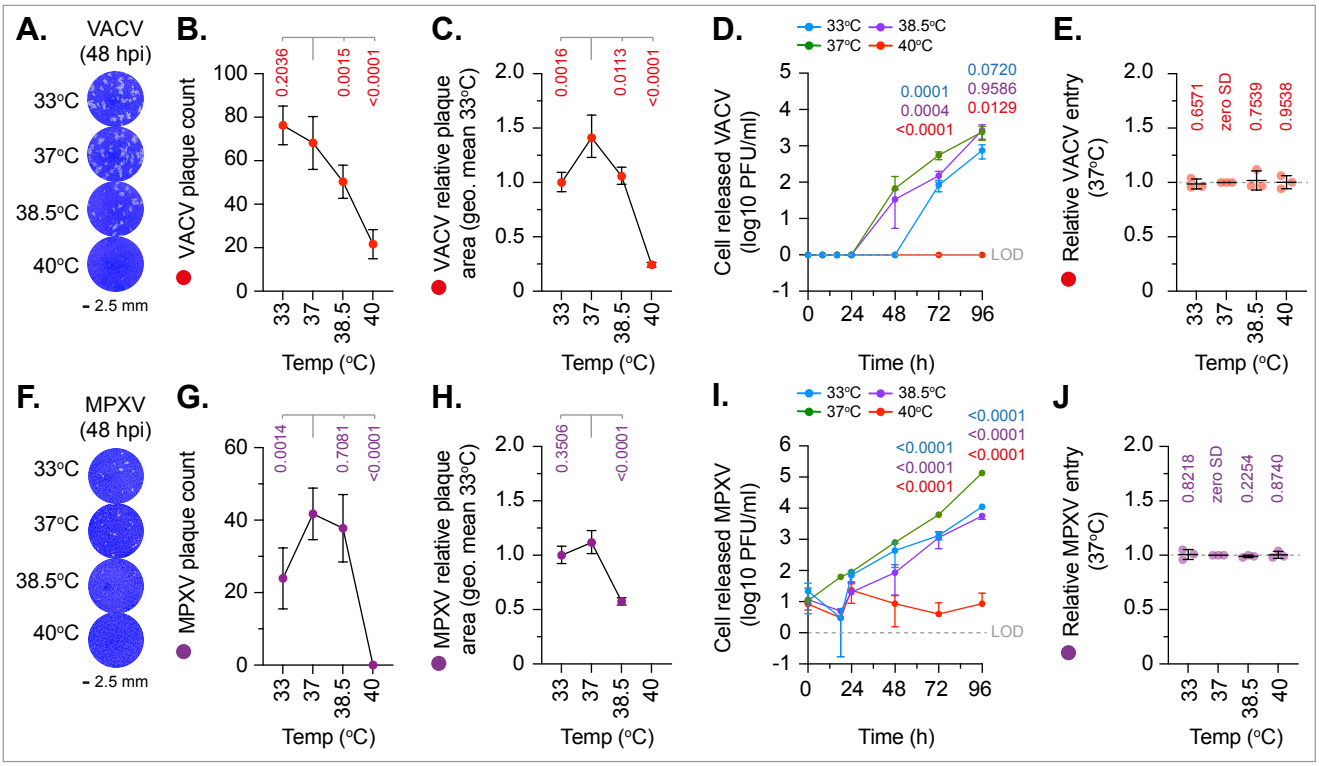

Figure 3. Temperature elevation inhibits MPXV replication

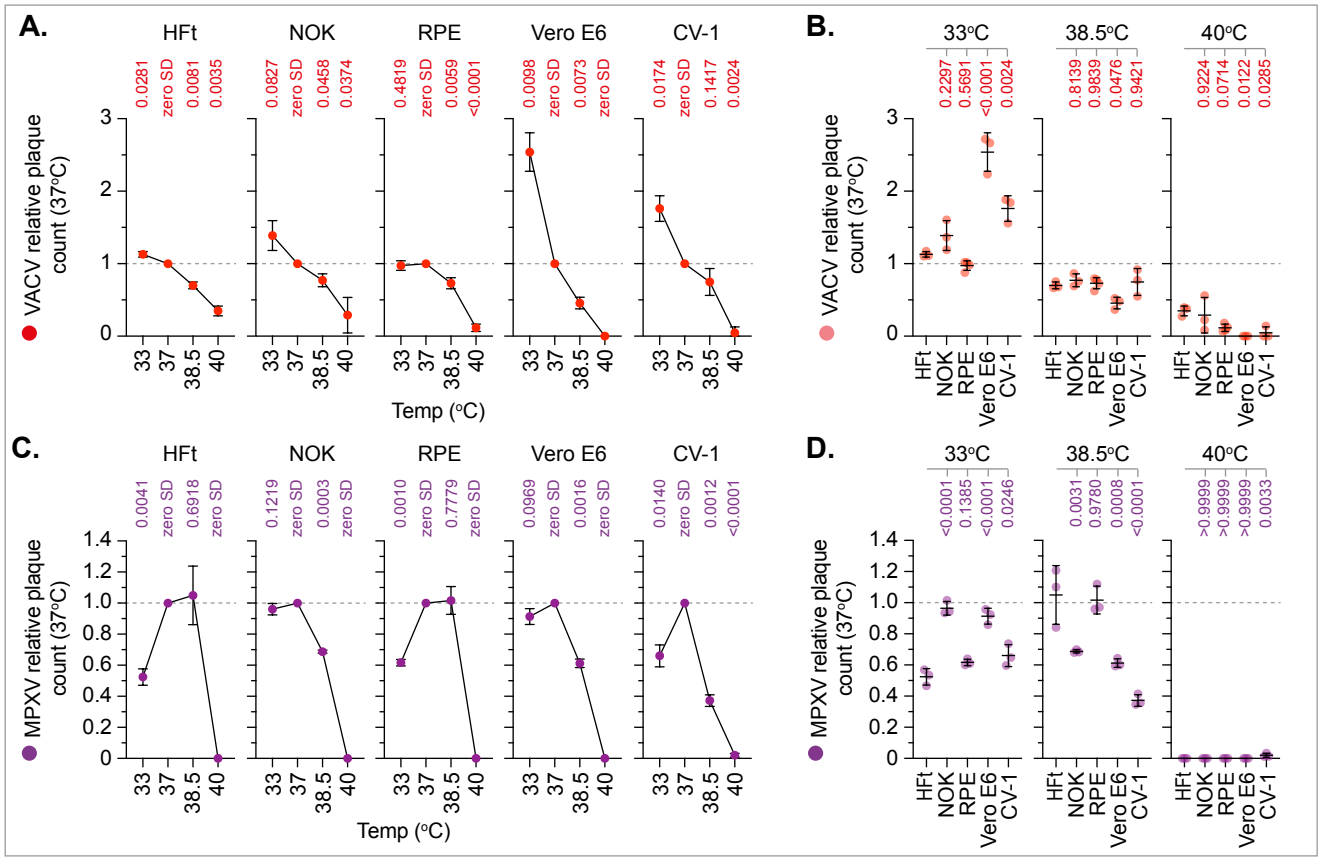

Figure 4. Basal host-cell temperature influences MPXV replication in a cell-type dependent manner

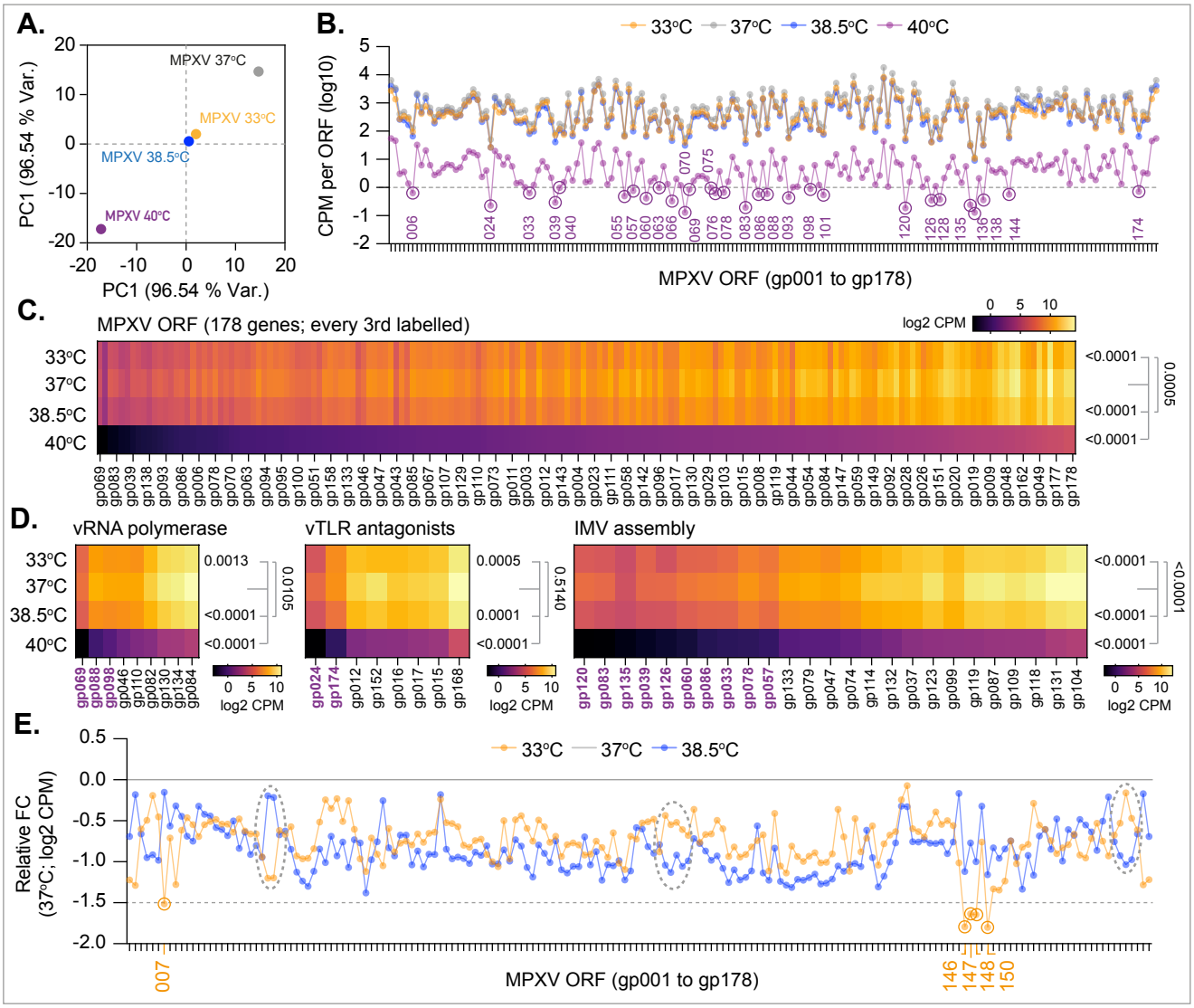

Figure 5. Basal host-cell temperature differentially influences the regulation of MPXV transcription

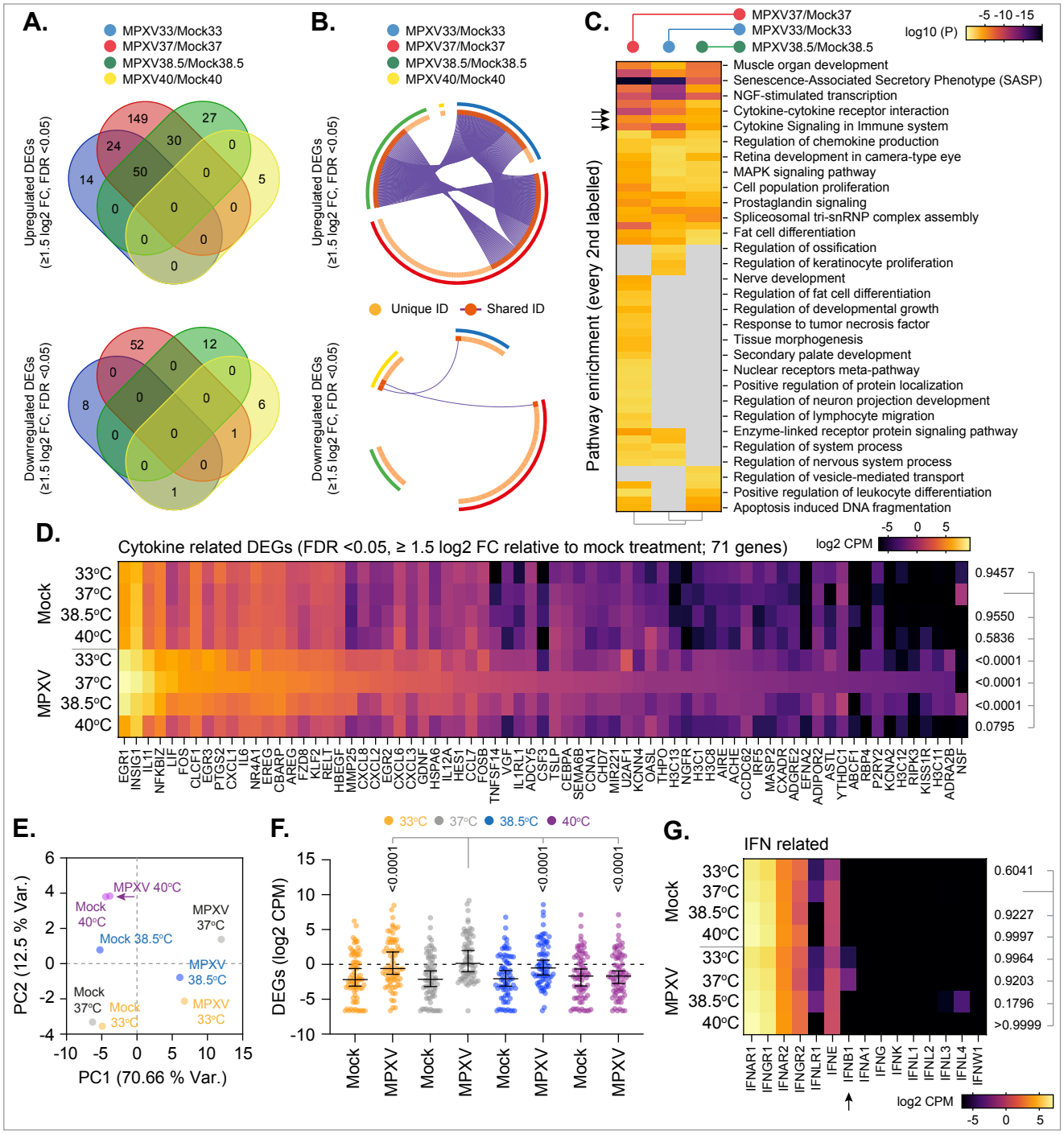

Figure 6: Basal temperature influences the host-cell response to MPXV infection

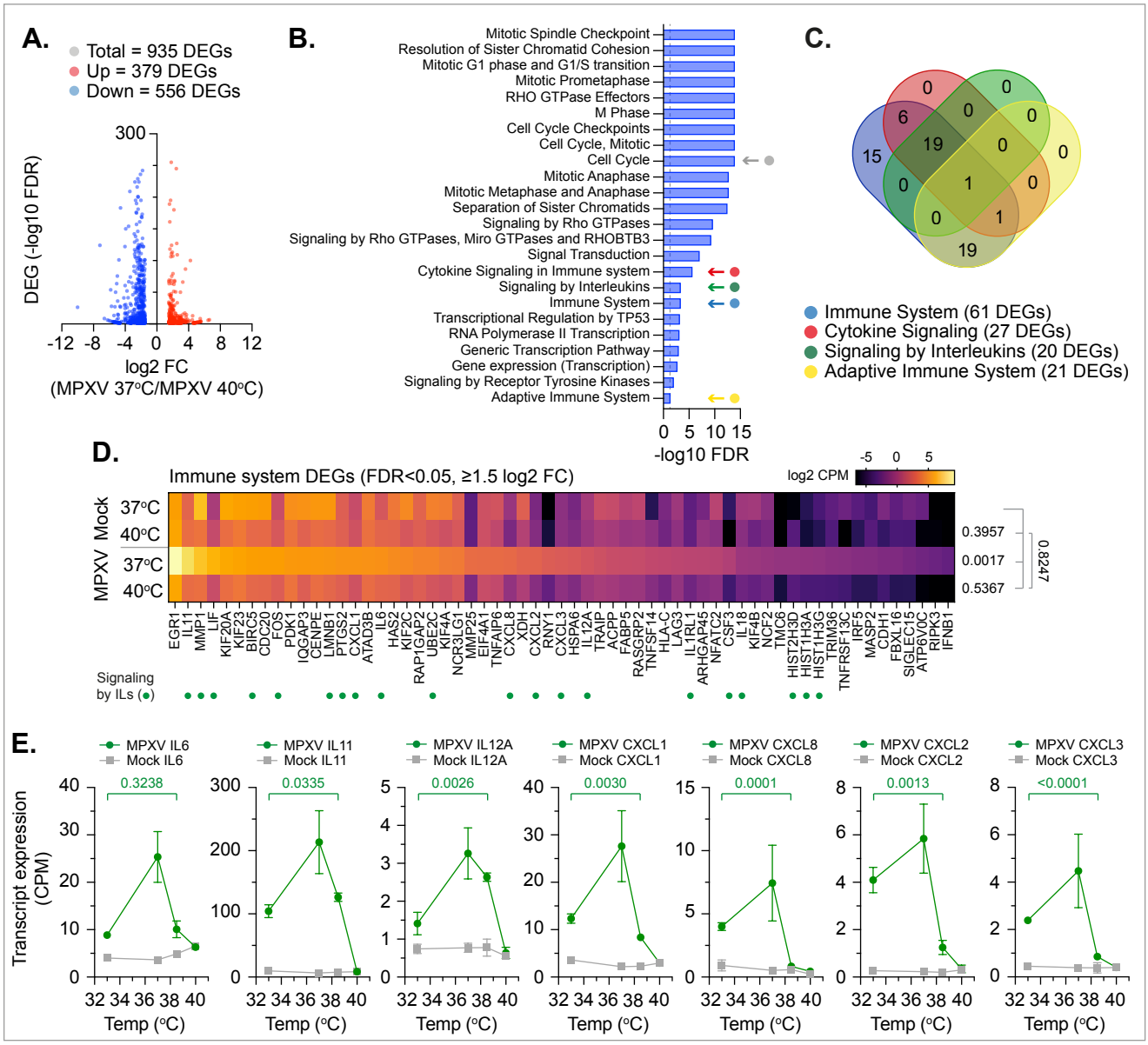

Figure 7: Basal host-cell temperature influences the interleukin response to MPXV infection

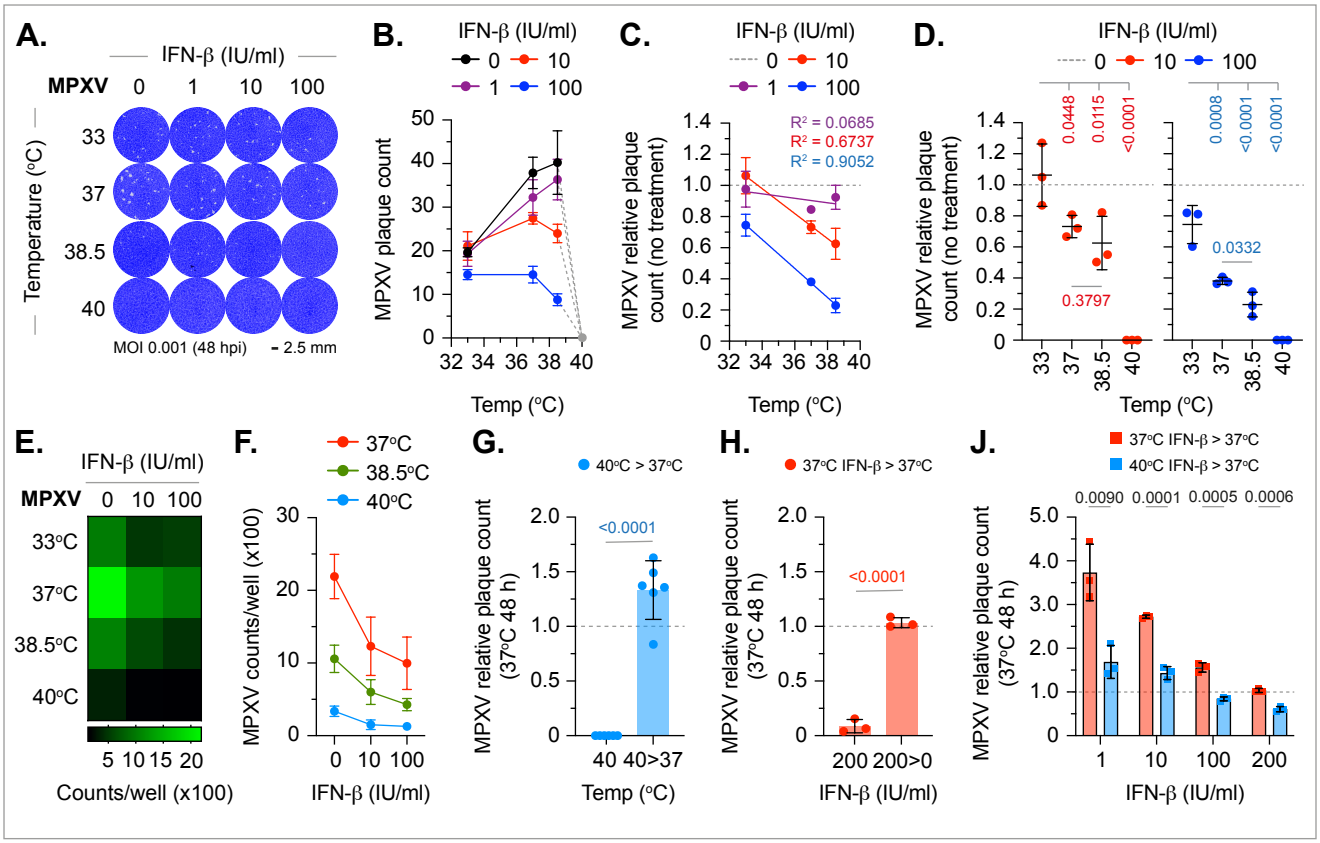

Figure 8: Temperature elevation enhances the type-I IFN-mediated host-cell restriction of MPXV

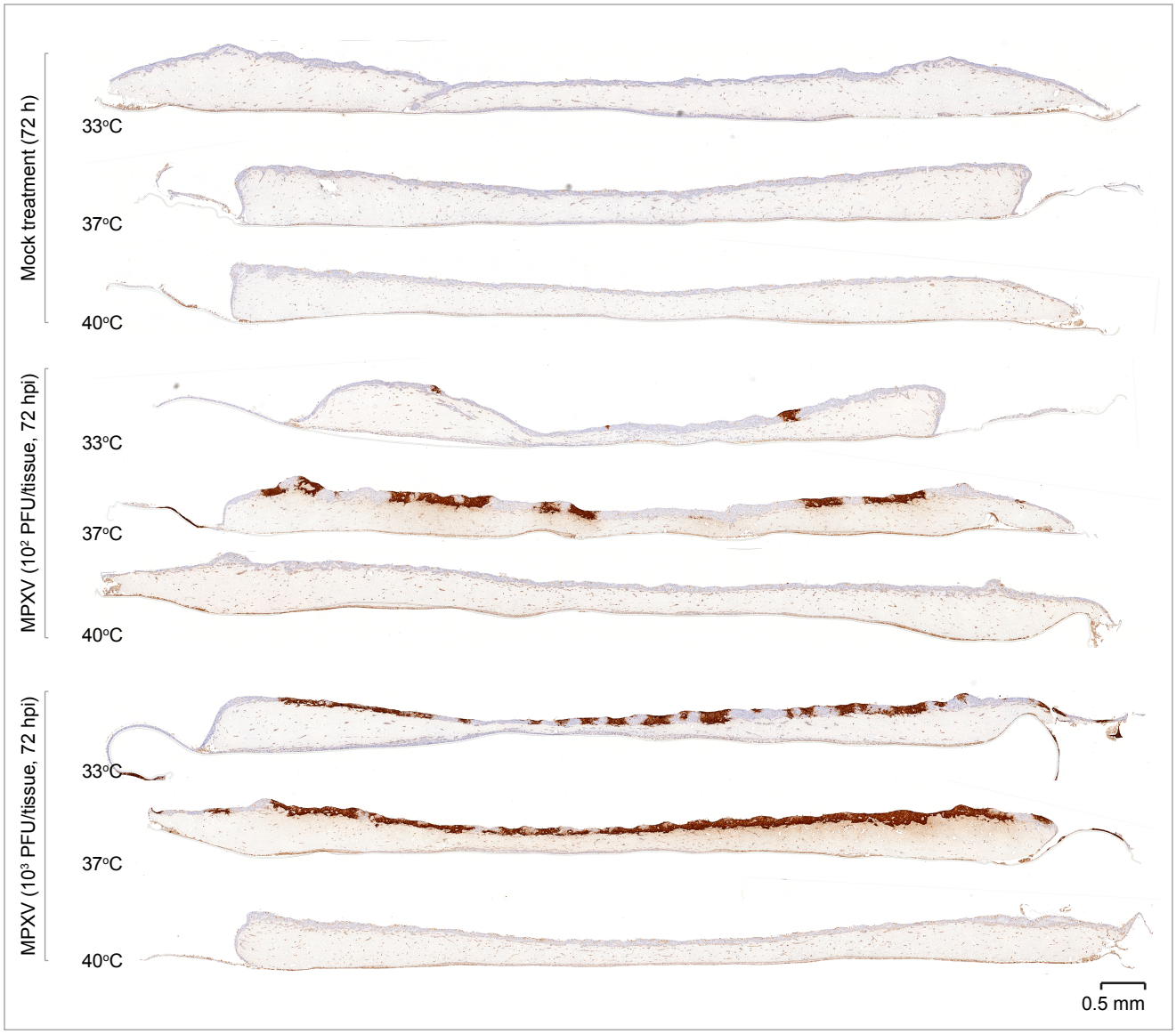

Figure S1. Tissue temperature influences the outcome of MPXV replication in skin epithelium

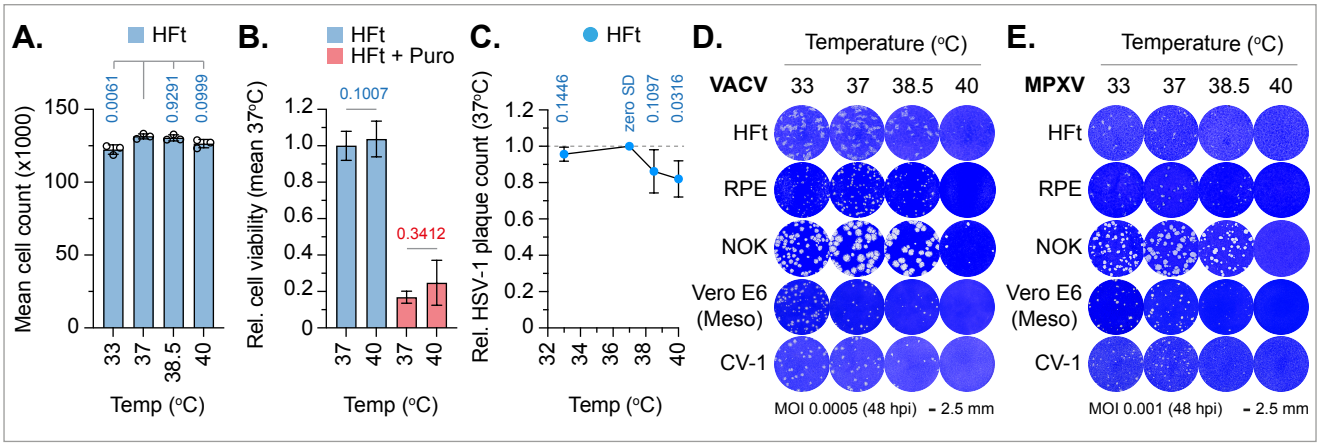

Figure S2. Temperature elevation inhibits orthopoxivurs replication.

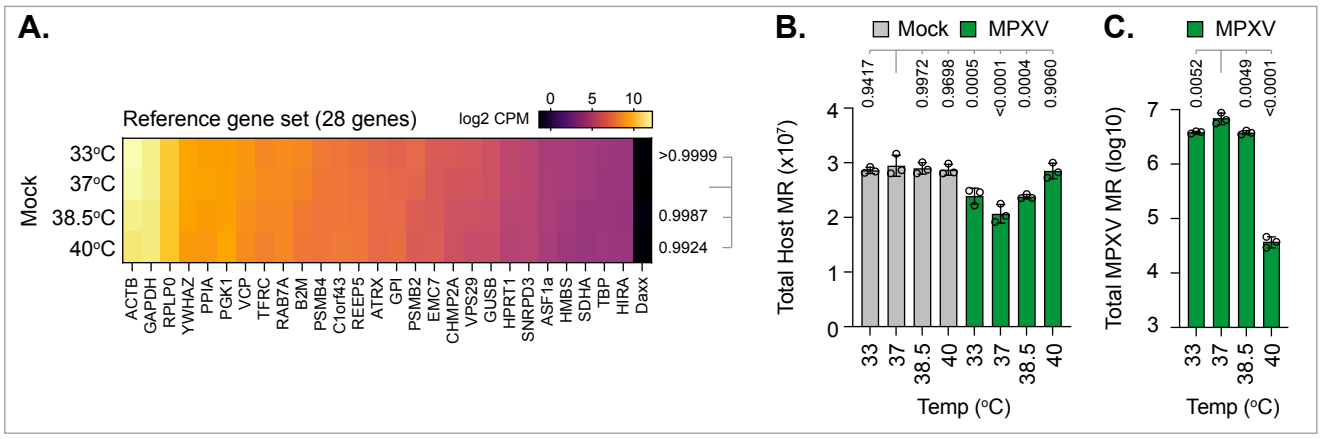

Figure S3: Basal host-cell temperature differentially influences MPXV transcription

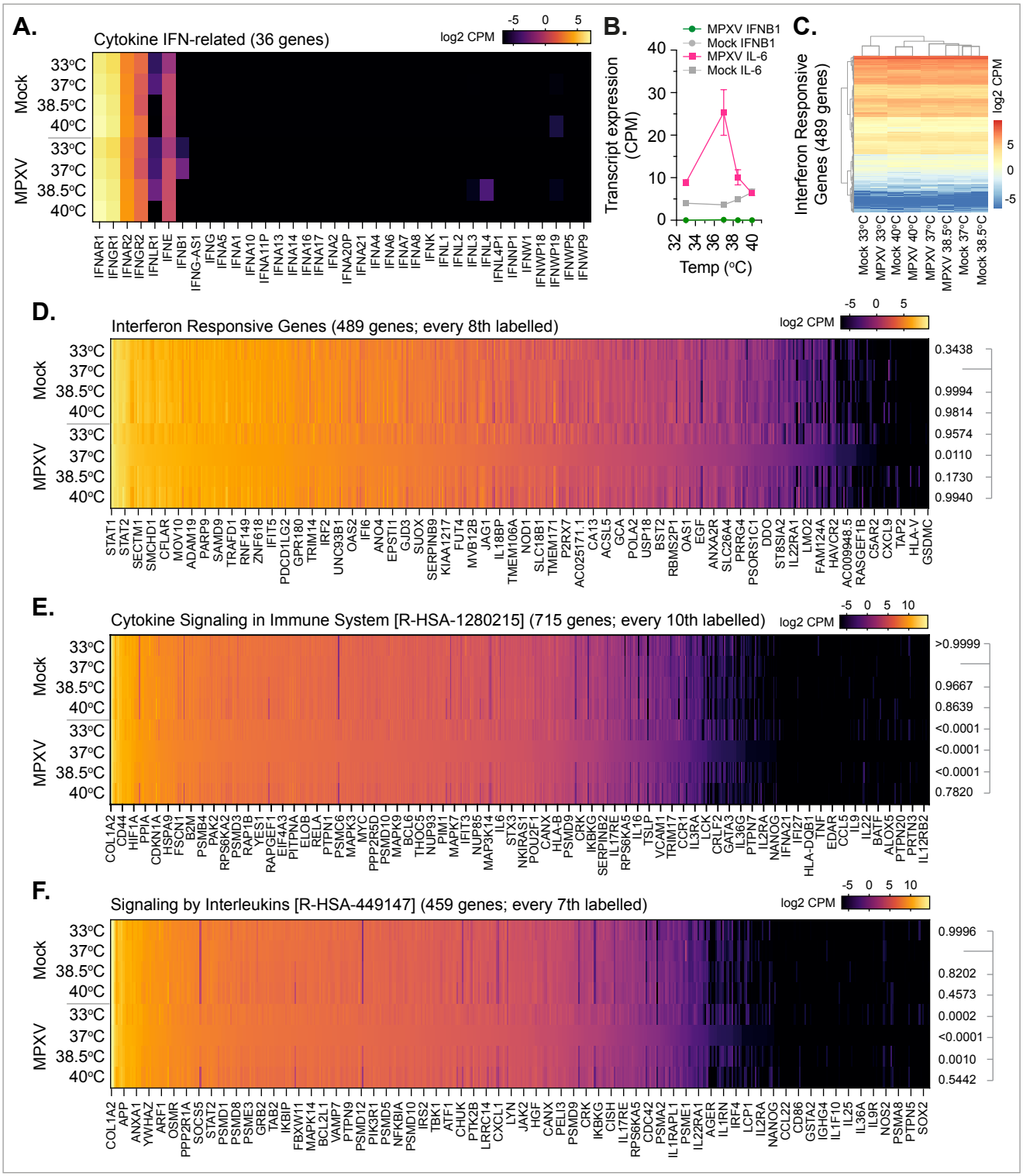

Figure S4. MPXV infection does not stimulate the induction of the type-I IFN respons

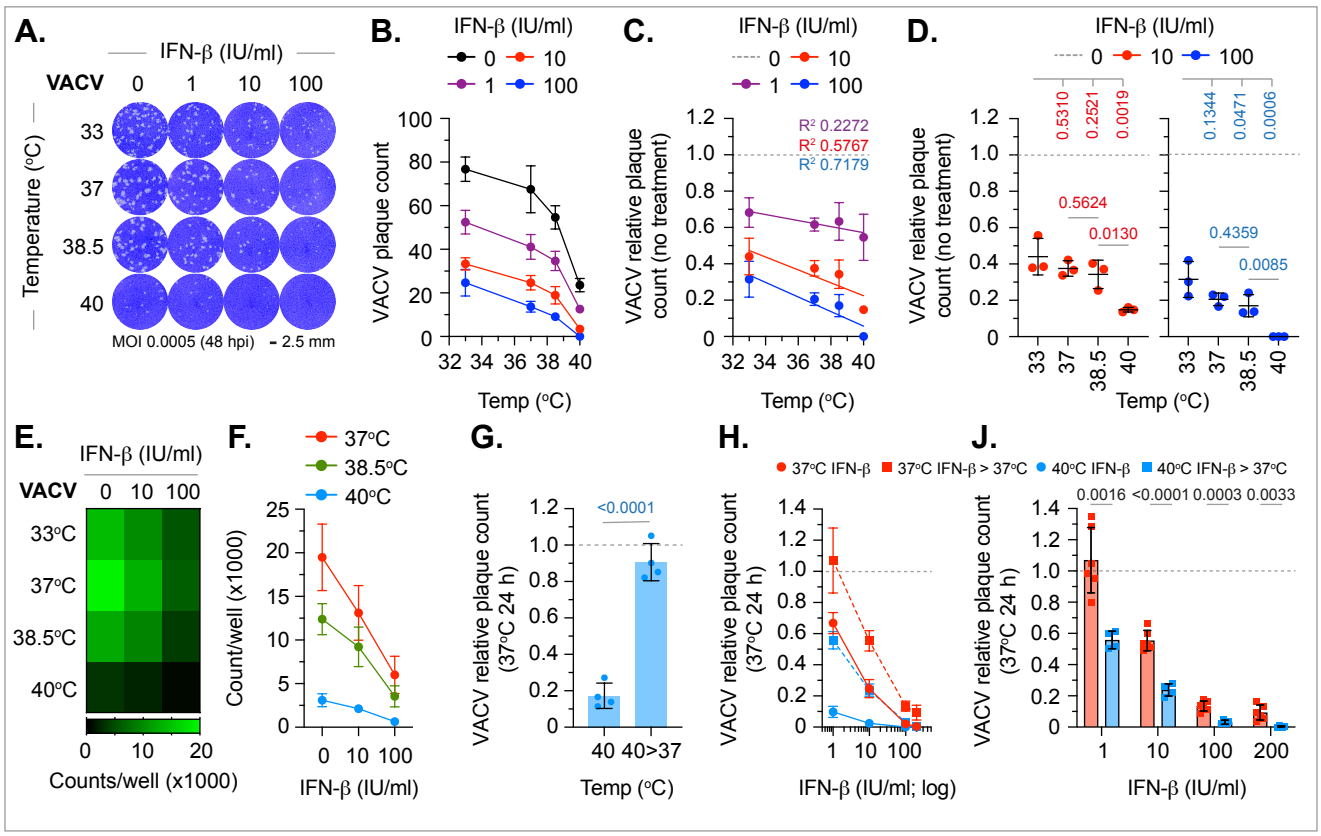

Figure S5. Temperature elevation enhances the type-I IFN-mediated host-cell restriction of VACV